Geophys. J. R. astr. Soc. (1987) **90**, 171–224

Glacial rebound and relative sea-level variations: a new appraisal

Masao Nakada and Kurt Lambeck *Research School of Earth Sciences, Australian National University, PO Box 4, Canberra, ACT 2601, Australia*

Accepted 1986 December 3. Received 1986 December 3; in original form 1986 July 21

Summary. Late Pleistocene and Holocene changes in sea-level at tectonically stable shorelines contain information on the melting history of the ice sheets and on the response of the Earth to changes in surface loads on time scales of 10^4 yr. Some separation of parameters defining the ice loads and the Earth's response can be achieved by examining sea-level change at different sites around the world and at different epochs. This paper examines the mathematical requirements for obtaining satisfactory solutions for the sea-level equation rather than emphasizing results for the Earth's response to the surface loads. An examination of the equation expressing the sea-level variation on a viscoelastic earth indicates that careful consideration needs to be given to both the definition of the ice load and the geometry of the redistributed water load if geophysically significant Earth-response parameters are to be deduced from observations of relative sea-level. The spectrum of the $5^\circ \times 5^\circ$ area-mean description of the ice load, widely used in glacial rebound studies, contains significant power at high degrees ($n > 30$) and can result in substantial spatial variations in sea-level unless a thick lithosphere is introduced in the Earth's response function. A smoothed $1^\circ \times 1^\circ$ description of the ice model avoids these high-degree oscillations in relative sea-level and produces satisfactory sea-level results without requiring a thick lithosphere. At far field sites, the Holocene sea-levels are sensitive to the Earth's response to the meltwater loading in the vicinity of the site and a high-degree spatial resolution of coastline geometry is required to model the mantle flow driven by the differential loading about the site. At some sites convergence of the solution to the sea-level equation is not obtained, even when the solution is expanded to degree 180. Convergent solutions at lower degrees can be achieved by introducing earth models with a moderately thick lithosphere. If high-resolution ice and meltwater load models are not used then the tendency will be to overestimate the effective elastic thickness of the lithosphere. Estimates of mantle viscosity are also of questionable value if these high resolution models are not used. A preliminary examination of sea-

levels at sites in both the near- and far-field places an upper limit of about 50–80 km on the effective lithospheric thickness. These sea-level observations are also consistent with an upper mantle viscosity of about 10^{21} Pa s with a lower mantle viscosity in the range of 10^{21}–10^{23} Pa s.

Key words: sea-level, glacial rebound, hydro-isostasy, mantle viscosity

1 Introduction

The observed variations in sea-level at continental shorelines and ocean islands have two principal causes: tectonic processes leading to subsidence or uplift of the shorelines, and changes in water volume or in the holding capacity of the oceans. The two contributions are effective on both geological and contemporary time scales. The major factor contributing to geologically recent changes in global sea-level has been the melting of the late Pleistocene ice sheets and the concomitant adjustment of the Earth's crust to the redistribution of the surface loads. Ignoring other geological processes that may change the water volume or the geometry of the ocean basins, observations of the rise and fall of sea-level relative to the crust provide a relation between three contributions: tectonic processes causing uplift or subsidence of the shorelines, the melting histories of the ice sheets, and the mechanical response of the Earth to the redistributed surface load of ice and meltwater. Glaciologists have used the sea-level information to constrain the volume of past ice sheets; tectonophysicists use the relative sea-level changes to examine the processes that deform the crust and lithosphere; geophysicists use the sea-level signatures to estimate the rheological properties of the mantle and the mechanical properties of the lithosphere. It may well be asked whether it is in fact possible to separate the various parameters defining the geometry of the ice load through time, the Earth's response to loading and any additional tectonic processes operating, particularly in view of the rather limited, in both space and time, information on the sea-level changes. Obviously some separation can be achieved by avoiding areas that are independently known to be subjected to tectonic upheavals. Further separation is possible by examining different parts of the sea-level curve, for example, pre-Holocene and Holocene sea-levels. Geographically widespread sea-level records, from sites near the ice load (the near-field) and from sites away from the ice load (the far-field) also contribute to the separation of the various parameters.

The subject of the glacial isostatic adjustment and associated sea-level change is one of the classical geophysical problems. Van Bemmelen & Berlage (1935), Haskell (1935, 1936, 1937), Vening Heinesz (1937) and Niskannen (1948) analysed the glacial rebound of Fennoscandia and, using apparent relaxation times deduced from sea-level changes near the centre of the former ice load, estimated an effective uniform mantle viscosity of about 10^{21} Pa s. Takeuchi & Hasegawa (1965), McConnell (1965, 1968), Lliboutry (1971), Walcott (1972, 1973, 1980) and Nakada (1983) amongst others have suggested that much of the deformation is concentrated in the upper mantle, and that the rebound can be mathematically represented by a model in which a channel of low viscosity, corresponding to the asthenosphere, lies beneath the lithosphere.

Sea-level changes in the far-field have been examined by geomorphologists and traditionally these results have been presented as a single eustatic sea-level curve (e.g. Fairbridge 1961; Shepard 1963). Bloom (1967) pointed out that sea-level change during the glaciation–deglaciation cycle would not be uniform in the far-field because of the response of the crust to the time-dependent meltwater load and this response is sometimes referred to as hydro-isostasy. An early analysis of regional variations in far-field sea-levels for mantle

viscosity was by Chappell (1974) (see also Chappell *et al.* 1982), and the first attempts at consistent global analyses of the far-field sea-levels were by Cathles (1975), Farrell & Clark (1976) and Clark, Farrell & Peltier (1978) (see also Peltier, Farrell & Clark 1978; Clark & Lingle 1979; Nakiboglu, Lambeck & Aharon 1983; Wu & Peltier 1983; Nakada 1986). Some of these studies have shown that sea-level changes in tectonically stable areas can be used to constrain both the rheological structure of the Earth's mantle and the melting histories of the polar ice caps; namely, the pre-Holocene sea-level change at far-field sites is sensitive to the melting histories (Nakiboglu *et al.* 1983) and the Holocene sea-level change is sensitive to the upper mantle rheology (Chappell *et al.* 1982; Nakada 1986).

In recent papers by Cathles (1980), Wu & Peltier (1983), Peltier (1984, 1985) and Sabadini, Yuen & Gasperini (1985), several geophysically important conclusions have been drawn from the rebound observations. They include: (i) that there is evidence for a thick, about 200 km, mechanical lithosphere overlying the mantle (Peltier 1984), (ii) that the average mantle viscosity is about 10^{21} Pa s and that there is little evidence for a major increase in viscosity from the upper to lower mantle (Cathles 1975; Wu & Peltier 1983), (iii) the rheology of the lower mantle is transient (Sabadini *et al.* 1985; Peltier 1985). The first conclusion is of interest because the response is for a duration of the stress cycle that lies between the time-scales that are characteristic of seismic and tectonic deformations of the lithosphere. The second conclusion is of relevance to discussions of mantle convection. From quite independent arguments Hager (1984) and Richards & Hager (1984) returned to an older suggestion that there is a substantial increase in viscosity across the 670 km discontinuity and this has led Peltier (1985) and Sabadini *et al.* (1985) to interpret the rebound data in terms of a transient mantle rheology.

We have two principal reasons for making yet another examination of the global variations in sea-level in response to the melting of the late Pleistocene ice sheets and for questioning the above conclusions. One reason is that the ability to separate the Earth's response from the melt history of the ice sheets needs further investigation before definitive statements about the mantle viscosity structure can be made. The second reason is that the previous solutions have some significant limitations that could lead to erroneous interpretations of the observations. The uncertainties in the knowledge of the ice volumes through time remain substantial. For example, the Laurentide model of Peltier & Andrews (1976) predicts a global eustatic sea-level rise of about 60 m. That of Paterson (1972) predicts a rise of between 56 and 76 m, and that of Denton & Hughes (1981) predicts a rise of between 62 m and 93 m. These differences can have a major influence on solutions for mantle viscosity and lithospheric strength. The uncertainty resulting from an inadequate knowledge of the Antarctic melting history is also important (e.g. Nakiboglu *et al.* 1983). One example, the variations in sea-level at Boston, USA (see Fig. 19b below), illustrates this problem well. This observation has played an important role in discussions of the rheology of the mantle (Cathles 1975; Wu & Peltier 1983; Sabadini *et al.* 1985; Peltier 1985). The site is near the edge of the Laurentide ice sheet at about 20 000 years before present (20 ka BP), at a time when glaciation was at its maximum. Sea-level variations at such sites are particularly sensitive to the choice of deglaciation model and are characterized by a non-monotonic behaviour: a lowering of sea-level from about 12 ka to 7 ka BP and a gradual rise from about 7 ka BP to the present. But this record, and similar records along the east coast of North America, may also be sensitive to the melting of the Antarctic ice sheet during the late glacial phase. This latter contribution at these sites is approximately equal to the eustatic sea-level change (equal to volume of Antarctic meltwater at time t divided by the ocean surface area) and amounts to about 30 m at 14 ka BP for the Antarctic ice model ANT 1 (see Section 3 below). The melting history of Antarctica remains poorly known

(Denton & Hughes 1981) and any results for mantle rheology are plagued by this uncertainty. Yet Sabadini *et al.* (1985) and Peltier (1985) neglected the Antarctic deglaciation history in their discussion of transient rheology. To estimate the rheological structure it is necessary to first select locations where sea-level changes are not overly sensitive to the deglaciation history models. Other locations can be found that are more sensitive to melt histories than to mantle viscosity (Lambeck & Nakada 1985). In particular, by examining the late glacial sea-level changes at far-field sites it is possible to obtain estimates of the total meltwater volumes. For example, Nakiboglu *et al.* (1983) estimated from sea-level records that a volume of about $9 \times 10^6\,\mathrm{km}^3$ of ice originated from the Antarctic ice sheet in late Pleistocene time, very similar to the amount estimated quite independently by Denton & Hughes (1981).

The numerical limitations of the current solutions are associated with the high spatial resolutions required for the descriptions of the ice and ocean functions that define the surface loads through time. Cathles (1975, 1980), Peltier & Andrews (1976) and Wu & Peltier (1983) have computed variations in sea-level based on a 5° grid description of the ice load at a number of time intervals. Cathles' analysis, carried out in the Legendre transform domain, required him to truncate the ocean function expansion at degree $N_{max} = 36$. This procedure is mathematically and physically reasonable but is it possible to obtain a converged solution for the sea-level variations with $N_{max} = 36$? Another question is whether an adequate spherical harmonic representation can be obtained by up to degree 36 from the 5° dataset. The N_{max} used in the formulation of Peltier & Andrews (1976) and Wu & Peltier (1983) is infinite but the resolution of the ice grid should be as small as possible so as to correspond to this value of N_{max}. Is the 5° model used by them adequate for this? There is a similar discretization problem for the coastlines. Peltier's ocean function definition is variable over the globe, ranging from about 5° to 20° (see, for example, fig. 2 of Wu & Peltier 1983). A number of observations suggest, however, that far-field variations in sea-level along continental shorelines or between nearby islands occur over distances that are less than these resolutions. Chappell *et al.* (1982), for example, investigated sea-level changes in northern Australia and found significant variation in the Holocene sea-levels along the coastline over distances of about 500 km. Similar variations along coastlines have been noted elsewhere; along Australia's southern and western margins (Belperio, Hails & Gostin 1983; Brown 1983), in the Cook Islands (Yonekura *et al.* 1984; Stoddard, Spencer & Scoffin 1985) and in Japan (Sugimura 1977). The Holocene high stands in the far-field are at most only a few metres above present sea-level, yet they can often be defined with considerable precision, and in order to examine these spatial variations the resolution of the ocean function may need to be increased beyond what has been used in past studies (Nakada 1986). For example, in a spherical harmonic expansion of a 1° spatial-resolution ocean function, islands, such as Tahiti and smaller, are not represented and any mantle flow from beneath the island to beneath the oceans, or vice versa, is not modelled. The islands are partially represented by harmonic expansions of ocean functions described by a 10′ grid, even when the expansion is carried out only to degree 180. Do the two spatial resolutions produce comparable sea-level fluctuations, in particular for Holocene time when sea-level changes are at most a few metres?

Estimates of mantle viscosity have usually been made on the assumption that the Earth can be characterized as a Maxwell body although non-linear rheological models have been examined by Post & Griggs (1973), Crough (1977), Yokokura & Saito (1978) and Nakada (1983). The flow laws for the mantle, appropriate for the time-scales and stress magnitudes that are typical of the rebound problem, remain obscure, however (Kaula 1980), and the observational evidence does not appear to be inconsistent with the linear models. Thus a

linear rheology is also assumed to be adequate in this paper. Only if such models lead to systematic disagreements with the observations will non-linear model be required.

In Section 2 of this paper the mathematical formulation of the sea-level equations is established. We use the spherical harmonic or spectral approach to solving the sea-level equation (see also Cathles 1975; Nakiboglu *et al.* 1983) rather than the finite element approach adopted by Peltier & Andrews (1976) and Wu & Peltier (1983). The former method does require that the solutions are carried out to a high wavenumber but both methods have potential difficulties with achieving adequate yet practical spatial descriptions of the ice and meltwater loads. An advantage of the spectral approach is that it is possible to examine the resolving power for the mantle response given the surface loads and an assumed linear rheology although we have not attempted to do this formally in this paper. Section 3 describes the load function; the ice models and the ocean functions. No attempts are made here to improve upon existing ice models for the Arctic and the adoption of two specific models (ARC 1 and ARC 2) is solely to examine the sensitivity of sea-level change to the choice of ice model. Approximate Antarctic ice models are also considered for the same purpose. Section 4 describes the Earth's response function to the surface loads and Section 5 summarizes briefly the observations of sea-level change that are used in the comparisons with theory in Section 7. The criteria for obtaining convergent solutions of the sea-level equation are examined in Section 6 and this section constitutes the principal part of the paper. One important conclusion reached is that both the ice and ocean functions need to be defined with much higher resolution that has hitherto been appreciated. Section 7 examines the sensitivity of relative sea-levels to Earth models and to melting histories. The essential conclusion here is that if uncertainties about the latter remain, observations of sea-level near the edge of the ice load do not provide good constraints on Earth structure.

2 Mathematical formulation of the sea-level equation

The mathematical formulation of the global change in sea-level caused by the exchange of mass between the ice sheets and the oceans has been formulated rigorously by Farrell & Clark (1976). These authors emphasized the significant contributions to sea-level made by the self-gravitational effects of the ice and water and their solution ensures that the ocean surface remains an equipotential surface at all times, that mass is conserved, as well as allowing for the deformation of the crust due to the redistribution of the surface ice and water loads. Their integral equation for the change in sea-level ζ can be written in the following form

$$\zeta(\theta, \lambda: t) = \rho_i \left(\iint_{ice} G(\alpha)\, \zeta_i(\theta', \lambda': t)\, dw - \left\langle \iint_{ice} G(\alpha)\, \zeta_i(\theta', \lambda': t)\, dw \right\rangle \right)$$

$$+ \rho_w \left(\iint_{ocean} G(\alpha)\, \zeta(\theta', \lambda': t)\, dw - \left\langle \iint_{ocean} G(\alpha)\, \zeta(\theta', \lambda': t)\, dw \right\rangle \right) - \frac{M_i}{A_o \rho_w} \tag{1}$$

$\zeta(\theta, \lambda: t)$ is the sea-level change, positive when sea-level rises, at a point of colatitude θ and longitude λ at time t. The integrals are over an area of the Earth defined by either the ice load or by the ocean function. $\zeta_i(\theta', \lambda': t)$ is the change in ice height at position θ', λ' at time t and its sign convention is illustrated in Fig. 1. M_i is the change in the total mass of the

ice at time t, positive for accretion and negative for melting, and

$$M_i(t) = \iint_{ice} \zeta_i(t)\, dw. \tag{2}$$

The densities of ice and water are denoted by ρ_i and ρ_w, respectively. The eustatic sea-level (ESL) ζ_e is given by the last term of equation (1), or

$$\zeta_e(t) = -\frac{\rho_i}{A_o \rho_w} \iint_{ice} \zeta_i(t)\, dw, \tag{3}$$

where A_o is the surface area of the oceans. This term represents the uniform rise in sea-level that would result if the meltwater is uniformly distributed over the oceans but such a surface would not be an equipotential and is not realised. The brackes $\langle\ \rangle$ denote the mean value of the enclosed function over the oceans. α is the geometrical angle between the point $P(\theta, \lambda)$ at which sea-level is evaluated and the position $P'(\theta', \lambda')$ of the load. The kernel function $G(\alpha)$ for a rigid earth is

$$G(\alpha) = \frac{3}{4\pi\bar{\rho}} \frac{1}{2 \sin(\alpha/2)}. \tag{4a}$$

For an elastic earth this function is

$$G(\alpha) = \frac{3}{4\pi\bar{\rho}} \left(\frac{1}{2 \sin(\alpha/2)} + \sum_{n=0}^{N_{max}} (k_n - h_n) P_n(\cos\alpha) \right). \tag{4b}$$

In these definitions $\bar{\rho}$ is the mean density of the Earth, $P_n(\cos\alpha)$ is the Legendre polynomial of degree n and k_n and h_n are the potential and radial deformation load Love numbers for an elastic earth. The first two terms of equation (1) represent the contributions to sea-level from the unloading of the ice sheets and the third and fourth terms represent the contributions from the loading of the oceans by the meltwater. The second and fourth terms ensure that the total mass of ice and meltwater is conserved.

To solve equation (1) the required input is (i) the spatial and temporal description of an ice model, (ii) a geometric description of the ocean surface, and (iii) a rheological model of the Earth through the kernel $G(\alpha)$. The equation can then be solved by an iterative procedure using the method outlined in Nakiboglu *et al.* (1983). The zero order solution of (1) is obtained if self-attraction and crustal deformation is ignored and the result is simply the eustatic sea-level $\zeta_e(t)$. An improved solution is obtained by substituting $\zeta_e(t)$ into the rhs of equation (1) and, with the kernel (4a), the sea-level change on a rigid earth $\zeta_R(\theta, \lambda: t)$ becomes

$$\zeta_R(\theta, \lambda: t) = \zeta_e(t)\,[1 + C_1(S_1 - \langle S_1 \rangle)] + C_2(S_2 - \langle S_2 \rangle), \tag{5}$$

where

$$C_1 = \frac{3\rho_w}{4\pi\bar{\rho}}, \quad C_2 = \frac{3\rho_i}{4\pi\bar{\rho}},$$

and

$$S_1(\theta, \lambda) = \iint_{ocean} \frac{dw}{2 \sin(\alpha/2)}, \quad S_2(\theta, \lambda: t) = \iint_{ice} \frac{\zeta_i(\theta', \lambda': t)}{2 \sin(\alpha/2)}\, dw. \tag{6}$$

Any further iteration for the rigid earth solution is not required as was shown by Nakiboglu *et al.* (1983) because the additional terms resulting from such an iteration are of the order $(C_1)^2$ or about 2×10^{-3}. This represents a contribution of 20 cm for a sea-level change of 100 m, negligible in view of the observational accuracies of both sea-level and the ice models. Even when the deformation of the Earth is considered, these secondary contributions remain small compared with $\zeta_e(t)$.

The next iteration follows by substituting equation (5) into the rhs of equation (1) and introducing the response of the planet to the surface load. With the kernels defined by equation (4b) this gives the sea-level change on an elastic earth. The sea-level change on a linear (Maxwellian) viscoelastic body is obtained by applying the correspondence principle (Bland 1960; Peltier 1974) to the elastic equation. The result is

$$\zeta(\theta, \lambda: t) = \zeta_R(\theta, \lambda: t) + (Z_1 - \langle Z_1 \rangle) + (Z_2 - \langle Z_2 \rangle), \tag{7}$$

where

$$Z_1 = C_2 \sum_{n=0}^{N_{max}} \iint_{ice} L^{-1}[(\tilde{k}_n - \tilde{h}_n)\,\tilde{\xi}_i(s)]\, P_n(\cos\alpha)\, dw \tag{8}$$

$$Z_2 = C_1 a \sum_{n=0}^{N_{max}} \iint_{ocean} \left(\iint_{ice} L^{-1}[(\tilde{k}_n - \tilde{h}_n)\,\tilde{\xi}_i(s)]\, dw \right) P_n(\cos\alpha)\, dw.$$

L^{-1} is the inverse Laplace transform, and $\sim$ indicates quantities that have been transformed into the Laplace domain. The parameter a is defined as

$$a = \frac{-\rho_i}{4\pi a_{00}\rho_w},$$

where a_{00} is the zero degree spherical harmonic coefficient of the ocean function [equation (27), below]. The term $(Z_1 - \langle Z_1 \rangle)$ in equation (7) represents the variation in sea-level

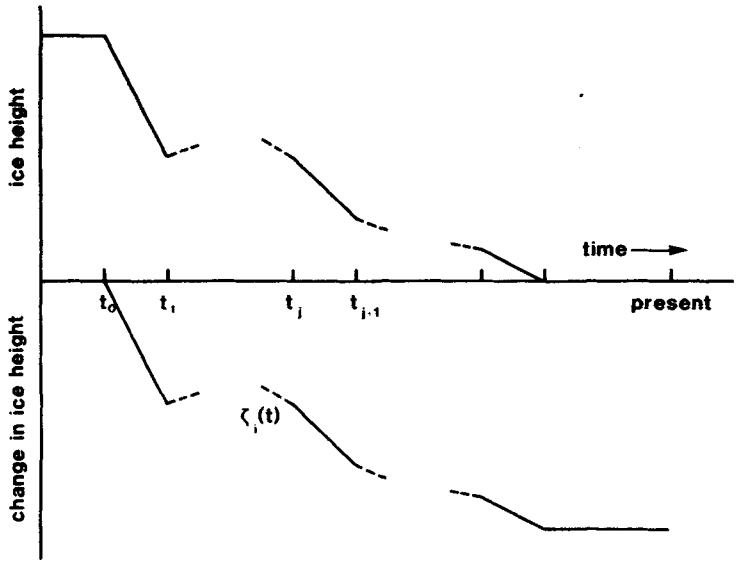

Figure 1. Sign convention for the change in ice height $\zeta_i(t)$ of an ice column at position θ', λ' at time t.

associated with the loading and unloading of the ice sheets and includes the effect of the self-attraction and the Earth's deformation. The term $(Z_2 - \langle Z_2 \rangle)$ represents the contribution to sea-level change caused by the loading or unloading of the meltwater. The terms $\langle Z_1 \rangle$ and $\langle Z_2 \rangle$ ensure that mass is conserved.

The sea-level equation (7) is essentially the same as that used by Farrell & Clark (1976) and Nakiboglu *et al.* (1983). The latter authors, however, made two assumptions to facilitate the computation of the inverse Laplace transforms in equation (7) but which could lead to misleading conclusions (Lambeck & Nakada 1985). First, it was assumed that in terms other than the eustatic term, the deglaciation history for any ice column between time t_0, the onset of deglaciation, and t_m, the end of deglaciation, is linear. Second, it was assumed that the start and end times of the deglaciation for all ice columns are the same.

In the present formulation the change in ice height for each ice column is assumed to be linear in the time interval between t_j and t_{j+1} (Fig. 1) and

$$\zeta_j(t) = a_j t + b_j, \quad t_j < t < t_{j+1}. \tag{9}$$

The entire melting history is defined by a total of r such intervals. With this definition the Laplace transform of $\zeta_i(t)$ is

$$\bar{\zeta}_i(\theta, \lambda: s) = \sum_{j=0}^{r} a_j \left(-\frac{t_{j+1}}{s} \exp(-st_{j+1}) - \frac{1}{s^2} \exp(-st_{j+1}) + \frac{t_j}{s} \exp(-st_j) + \frac{1}{s^2} \exp(-st_j) \right)$$
$$+ \sum_{j=0}^{r} b_j \left(-\frac{1}{s} \exp(-st_{j+1}) + \frac{1}{s} \exp(-st_j) \right),$$

where s is the Laplace transform parameter. Then

$$(\bar{k}_n - \bar{h}_n)\, \bar{\zeta}_i(\theta, \lambda: s) = \sum_{j=0}^{r} \frac{a_j(\bar{k}_n - \bar{h}_n)}{s} \left(-t_{j+1} \exp(-st_{j+1}) - \frac{1}{s} \exp(-st_{j+1}) \right.$$
$$\left. + t_j \exp(-st_j) + \frac{1}{s} \exp(-st_j) \right) + \sum_{j=0}^{r} \frac{b_j(\bar{k}_n - \bar{h}_n)}{s}$$
$$\times \left[-\exp(-st_{j+1}) + \exp(-st_j) \right]. \tag{10}$$

As was shown by Peltier (1974, p. 660), the $\bar{k}_n - \bar{h}_n$ can be quite adequately expanded numerically into the following form

$$(\bar{k}_n - \bar{h}_n) = \sum_{i=1}^{m} \frac{c_n^i}{s + s_i} + (k_n^e - h_n^e), \tag{11}$$

where k_n^e and h_n^e are the elastic load Love numbers. Equation (11) is essentially an eigenfunction expansion of the Love numbers and the s_i correspond to the eigenvalues. The inverse transform of (11) is simply

$$L^{-1}\left[\frac{\bar{k}_n - \bar{h}_n}{s} \right] = \sum_{i=1}^{m} \frac{c_i^n}{s_i} \left[1 - \exp(-s_i t) \right] + (k_n^e - h_n^e).$$

Also

$$L^{-1}\left(-t_{j+1} \exp(-st_{j+1}) - \frac{1}{s} \exp(-st_{j+1}) + t_j \exp(-st_j) + \frac{1}{s} \exp(-st_j) \right)$$
$$= t_j \delta(t - t_j) - t_{j+1}\, \delta(t - t_{j+1}) + H(t - t_j) - H(t - t_{j+1}) \tag{12a}$$

and

$$L^{-1}\,[-\exp(-st_{j+1})+\exp(-st_j)] = \delta(t-t_j)-\delta(t-t_{j+1}), \tag{12b}$$

where $\delta(t)$ and $H(t)$ are the delta and Heaviside unit step functions, respectively. With the definitions

$$\tilde{A}_j = \frac{\tilde{k}_n-\tilde{h}_n}{s}\left(-t_{j+1}\exp(-st_{j+1})-\frac{1}{s}\exp(-st_{j+1})+t_j\exp(-st_j)+\frac{1}{s}\exp(-st_j)\right)$$

and

$$\tilde{B}_j = \frac{\tilde{k}_n-\tilde{h}_n}{s}\,[-\exp(-st_{j+1})+\exp(-st_j)],$$

the analytical inverse transforms of these relations are, with Borel's theorem,

$$A_j = L^{-1}[\tilde{A}_j] = \begin{cases} 0, & t < t_j \\ \displaystyle\sum_{i=1}^{m}\frac{c_n^i}{s_i}\left[\left(\frac{1}{s_i}-t_j\right)\exp[-s_i(t-t_j)] + \left(t-\frac{1}{s_i}\right)\right] + (k_n^e-h_n^e)\,t, & t_j \leqslant t \leqslant t_{j+1} \\ \displaystyle\sum_{i=1}^{m}\frac{c_n^i}{s_i}\exp[-s_i(t-t_{j+1})]\left[\left(t_{j+1}-\frac{1}{s_i}\right) + \left(\frac{1}{s_i}-t_j\right)\exp[-s_i(t_{j+1}-t_j)]\right], & t > t_{j+1} \end{cases} \tag{13}$$

and

$$B_j = L^{-1}[\tilde{B}_j] = \begin{cases} 0 & t < t_j \\ \displaystyle\sum_{i=1}^{m}\frac{c_n^i}{s_i}[\![1-\exp[-s_i(t-t_j)]]\!] + (k_n^e-h_n^e) & t_j \leqslant t \leqslant t_{j+1} \\ \displaystyle\sum_{i=1}^{m}\frac{c_n^i}{s_i}\exp[-s_i(t-t_{j+1}]\;[\![1-\exp[-s_i(t_{j+1}-t_j)]]\!]. & t > t_{j+1} \end{cases} \tag{14}$$

We define the following functions in equation (8)

$$I_n = \iint_{\text{ice}} L^{-1}[(\tilde{k}_n-\tilde{h}_n)\,\tilde{\xi}_i(s)]\;P_n(\cos\alpha)\,dw$$

$$J_n = \iint_{\text{ocean}}\left(\iint_{\text{ice}} L^{-1}[(\tilde{k}_n-\tilde{h}_n)\,\tilde{\xi}_i(s)]\;dw\right)P_n(\cos\alpha)\,dw \tag{15}$$

and

$$Q_n(\theta,\lambda\colon t) = L^{-1}[(\tilde{k}_n-\tilde{h}_n)\,\tilde{\xi}_i(\theta,\lambda\colon s)]. \tag{16}$$

This last function can be written as [with equations (13) and (14)]

$$Q_n(\theta, \lambda: t) = \sum_{j=1}^{r} (a_j A_j + b_j B_j) \tag{17}$$

so that

$$I_n = \iint_{\text{ice}} Q_n(\theta', \lambda': t)\, P_n(\cos\alpha)\, dw, \tag{18}$$

and

$$J_n = \iint_{\text{ocean}} F_n(t)\, P_n(\cos\alpha)\, dw, \tag{19}$$

where

$$F_n(t) = \iint_{\text{ice}} Q_n(\theta', \lambda': t)\, dw. \tag{20}$$

The resulting solution for the sea-level equation (7) can now be written as

$$\begin{aligned}\zeta(\theta, \lambda: t) = \zeta_R(\theta, \lambda: t) + C_2 \sum_{n=0}^{N_{\max}} \Bigg(& \iint_{\text{ice}} Q_n(\theta', \lambda': t)\, P_n(\cos\alpha)\, dw \\ & - \left\langle \iint_{\text{ice}} Q_n(\theta', \lambda': t)\, P_n(\cos\alpha)\, dw \right\rangle \Bigg) \\ & + C_1 a \sum_{n=0}^{N_{\max}} F_n(t) \left(\iint_{\text{ocean}} P_n(\cos\alpha)\, dw - \left\langle \iint_{\text{ocean}} P_n(\cos\alpha)\, dw \right\rangle \right).\end{aligned} \tag{21}$$

With equations (5) and (7) the sea-level equation (21) is

$$\zeta(\theta, \lambda: t) = \zeta_e(t)\, [1 + C_1(S_1 - \langle S_1 \rangle)] + C_2(S_2 - \langle S_2 \rangle) + (Z_1 - \langle Z_1 \rangle) + (Z_2 - \langle Z_2 \rangle). \tag{22}$$

The numerical evaluation of the various terms in equation (22) requires some attention to ensure that adequate precision is maintained. The term $Z_1(\theta, \lambda: t)$ can be written as

$$\begin{aligned}Z_1(\theta, \lambda: t) = C_2 \sum_{n=0}^{N_{\max}} \frac{1}{2n+1} \sum_{m=0}^{n} \iint_{\text{ice}} Q_n(\theta', \lambda': t)\, [\![P_n^m(\cos\theta)\, P_n^m(\cos\theta') \\ \times [\cos m\lambda \cos m\lambda' + \sin m\lambda \sin m\lambda']]\!]\, dw,\end{aligned} \tag{23}$$

where the $P_n^m(\cos\theta)$ are fully normalized spherical functions of degree n and order m. The function Q_n can be expanded into spherical harmonics as

$$Q_n = \sum_{m=0}^{n} [H'_{nm}(t) \cos m\lambda + H''_{nm}(t) \sin m\lambda]\, P_n^m(\cos\theta)$$

with

$$\begin{bmatrix} H'_{nm}(t) \\ H''_{nm}(t) \end{bmatrix} = \frac{1}{4\pi} \iint_{\text{Earth}} Q_n(\theta, \lambda: t)\, P_n^m(\cos\theta) \begin{bmatrix} \cos m\lambda \\ \sin m\lambda \end{bmatrix} dw. \tag{24}$$

Then, because this function is zero outside the ice sheet

$$Z_1(\theta, \lambda: t) = C_2 \sum_{n=0}^{N_{max}} \frac{4\pi}{2n+1} \sum_{m=0}^{n} [H'_{nm}(t) \cos m\lambda + H''_{nm}(t) \sin m\lambda] P_n^m(\cos\theta). \tag{25}$$

The term $\langle Z_1 \rangle$ represents the average value of Z_1 over the oceans where

$$\langle Z_1 \rangle = \frac{C_2}{a_{00}} \sum_{n=0}^{N_{max}} \frac{1}{2n+1} \sum_{m=0}^{n} \left(H'_{nm}(t) \iint_{ocean} P_n^m(\cos\theta) \cos m\lambda \, dw \right.$$

$$\left. + H''_{nm}(t) \iint_{ocean} P_n^m(\cos\theta) \sin m\lambda \, dw \right).$$

Introducing the ocean function

$$O(\theta, \lambda) = \begin{cases} 1, \text{ where there is ocean} \\ 0, \text{ where there is land} \end{cases} \tag{26}$$

and expanding this as

$$O(\theta, \lambda) = \sum_n \sum_m (a_{nm} \cos m\lambda + b_{nm} \sin m\lambda) P_n^m(\cos\theta) \tag{27}$$

the term $\langle Z_1 \rangle$ reduces to

$$\langle Z_1 \rangle = C_2 \sum_{n=0}^{N_{max}} \frac{4\pi}{(2n+1)a_{00}} \sum_{m=0}^{n} [a_{nm} H'_{nm}(t) + b_{nm} H''_{nm}(t)]. \tag{28}$$

The term Z_2, defined as

$$Z_2(\theta, \lambda: t) = C_1 a \sum_{n=0}^{N_{max}} F_n(t) \iint_{ocean} P_n(\cos\alpha) \, dw, \tag{29}$$

can be transformed into a similar form, using the expansion (27) of the ocean function, as

$$Z_2(\theta, \lambda: t) = C_1 a \sum_{n=0}^{N_{max}} \frac{4\pi}{2n+1} F_n(t) \sum_{m=0}^{n} (a_{nm} \cos m\lambda + b_{nm} \sin m\lambda) P_n^m(\cos\theta). \tag{30}$$

and $\langle Z_2 \rangle$ follows as

$$\langle Z_2 \rangle = C_1 a \sum_{n=0}^{N_{max}} \frac{4\pi}{a_{00}(2n+1)} F_n(t) \sum_{n=0}^{m} (a_{nm}^2 + b_{nm}^2), \tag{31}$$

where $\Sigma_n(a_{nm}^2 + b_{nm}^2)$ is the power spectrum of the ocean function (26).

The other terms required in equation (22) are S_1 and S_2 (equation 6). The first can be written as

$$S_1(\theta, \lambda) = \sum_{n=0}^{N_{max}} \iint_{ocean} P_n(\cos\alpha) \, dw$$

$$= \sum_{n=0}^{N_{max}} \frac{4\pi}{2n+1} \sum_{m=0}^{n} (a_{nm} \cos m\lambda + b_{nm} \sin m\lambda) P_n^m(\cos\theta). \tag{32}$$

Also

$$\langle S_1 \rangle = \sum_{n=0}^{N_{max}} \frac{4\pi}{a_{00}(2n+1)} \sum_{m=0}^{n} (a_{nm}^2 + b_{nm}^2). \tag{33}$$

The ice function ζ_i in the integral of S_2 (equation 6) is expanded in spherical harmonics as

$$\zeta_i(\theta, \lambda: t) = \sum_{n=0}^{N_{max}} \sum_{m=0}^{n} [h'_{nm}(t) \cos m\lambda + h''_{nm}(t) \sin m\lambda] P_n^m(\cos\theta)$$

with

$$\begin{bmatrix} h'_{nm}(t) \\ h''_{nm}(t) \end{bmatrix} = \frac{1}{4\pi} \iint_{\text{Earth}} \zeta_i(\theta, \lambda: t) P_n^m(\cos\theta) \begin{bmatrix} \cos m\lambda \\ \sin m\lambda \end{bmatrix} dw. \tag{34}$$

Then, because $\zeta_i(\theta, \lambda: t)$ is zero outside the ice sheets,

$$S_2(\theta, \lambda: t) = \sum_{n=0}^{N_{max}} \frac{4\pi}{2n+1} \sum_{m=0}^{n} [h'_{nm}(t) \cos m\lambda + h''_{nm}(t) \sin m\lambda] P_n^m(\cos\theta) \tag{35}$$

and

$$\langle S_2 \rangle = \sum_{n=0}^{N_{max}} \frac{4\pi}{a_{00}(2n+1)} \sum_{m=0}^{n} [a_{nm} h'_{nm}(t) + b_{nm} h''_{nm}(t)]. \tag{36}$$

Equations (25), (28), (30)–(33), (35) and (36) are numerically evaluated once the ocean function and ice loads are specified.

3 Ice models and ocean functions

ICE MODELS

The details of the deglaciation history of the polar caps are important in obtaining satisfactory solutions for the global sea-level variations, not only for sites near the edges of the ice sheets (e.g. Quinlan & Beaumont 1981, 1982; Wu & Peltier 1983) but also for sites in the far-field (Nakiboglu *et al.* 1983). The Arctic ice sheets have been much studied, most recently by Denton & Hughes (1981) but for the present study we adopt the model of Peltier & Andrews (1976), referred to by them as ICE 1 but referred to here as ARC 1 as it describes the Arctic ice sheet only. This model has been used in a number of recent glacial rebound studies although it is known to have some defects, particularly at the edges of the ice sheets (e.g. Quinlan & Beaumont 1981; Wu & Peltier 1983). It is, however, based wholly on glacialogical and geomorphological observations and arguments and has not been adjusted to fit spatial variations in sea-level. A second model, ICE 2, of Wu & Peltier (1983) is also used for purposes of comparison. This is a modification of ICE 1, adjusted to make the predicted rebound consistent with some observations of sea-level change and is therefore partly dependent on the rheological model assumed. Both models are defined by the heights of columns of ice of 5° latitude by 5° longitude extent at a number of epochs. ICE 2 does include a melt component from Antarctica. In this study, only the Arctic part of the original ICE 2 model is considered and this is referred to here as ARC 2. A principal difference between the two Arctic ice models occurs in the melting rates in the central region of the Laurentide ice sheet during the early stages of deglaciation; the rates are higher for ARC 2 than for ARC 1 (Fig. 2; see also Fig. 18). A second difference occurs in the maximum ice

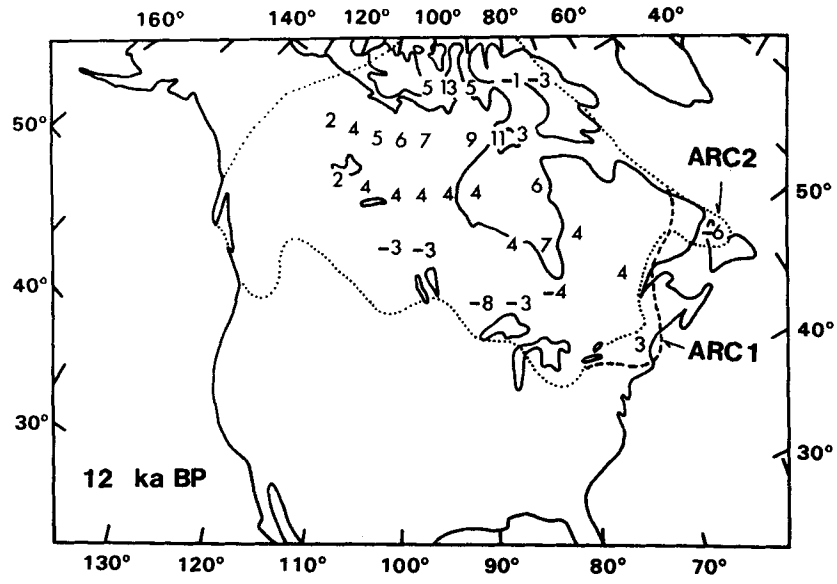

Figure 2. Extent of the two Laurentide ice sheet models ARC 1 and ARC 2 at 12 ka BP and the differences (ARC 1–ARC 2) in ice thickness of 5° by 5° ice columns (in units of 100 m) between the two models at this time.

thickness of the Fennoscandian ice sheet, it being about 25 per cent thinner for ARC 2 than for ARC 1. Other differences occur along the edge of the ice sheet at its maximum extent. While such differences may be minor from a global glacialogical viewpoint they are significant in terms of the predicted sea-level changes near the edge of the ice sheet (see also Peltier & Andrews 1976; Quinlan & Beaumont, 1981, 1982; Wu & Peltier 1983).

The use of the ICE 2 model of Wu & Peltier does raise the possibility of a circular argument. These authors 'modify the ice history to remedy local errors in relative sea-level fits to the predictions of the 10^{21} Pa s uniform mantle viscosity model and of fits to the free air gravity observations' (Wu & Peltier 1983, p. 408). A lithospheric thickness of 120 km has also been assumed (p. 401). They do not state which relative sea-level observations have been used in this iterative process and the presumption here is that observations such as those illustrated in their figs 14–19 have been used. This interpretation is partly influenced by their modifications of the melting rates of the edges of the ice sheets in Newfoundland and Nova Scotia, for example, where the changes are similar to those proposed by Quinlan & Beaumont (1982) which are based on sea-level data from the edge of the ice sheet.

The late Pleistocene changes in the Antarctic ice sheet are less well-known than in their northern counterpart and in particular the times of onset and end of deglaciation are poorly known. We adopt here the difference between the maximum late Pleistocene reconstruction of Denton & Hughes (1981, p. 269) and the present ice thickness as given by Drewry (1982) and, for want of further precise information, the melting history of each column of 5° x 5° extent is arbitrarily assumed to be synchronous with the ESL variation corresponding to ice model ARC 2. (ARC 2 was initially chosen because it was thought to be superior to ARC 1 but this choice is not significant for defining the Antarctic model.) This Antarctic ice melting model is referred to as model ANT 1. Stuiver *et al.* (1981, p. 414 *et seq.*) favour a model similar to ANT 1 in which melting occurred primarily between about 17 and 6.7 ka BP with a significant fraction of the total melting having occurred after 12 ka BP (see also

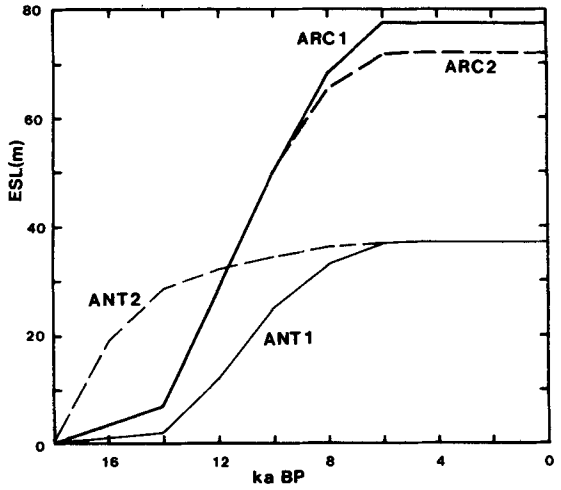

Figure 3. Eustatic sea-level (ESL) – see equation (3) – corresponding to the two Arctic models, ARC 1 and ARC 2, and to the two Antarctic models, ANT 1 and ANT 2, during the last 18 000 yr.

Broecker 1984). A second model ANT 2 is also considered in which the ice volume is the same as ANT 1 but for which the melting of each ice column is assumed to be synchronous with the ESL of the Antarctic part of the original model of Wu & Peltier (1983). Fig. 3 illustrates the eustatic sea-levels for the various melting histories adopted. In the ANT 2 model the start of deglaciation is significantly earlier than it is for both the ANT 1 and the Arctic models and if this is correct then the Antarctic contribution to Holocene sea-level change is minimal. These Arctic and Antarctic models cover the likely range of melting histories of the late Pleistocene ice sheets and they should suffice to evaluate the dependence of sea-level variations and of inferred viscosity models to the choice of ice model.

Fig. 4(a) illustrates the power spectra of the differential ice thickness between 18 ka BP and the present for the models ARC 1 and ANT 1. For $5^\circ \times 5^\circ$ area means in polar regions the power spectrum will exhibit considerable power at degrees higher than 36 and this is illustrated by the comparison of the 5° spectra with those based on $1^\circ \times 1^\circ$ area mean-values that have been linearly interpolated from the 5° model such that mass is conserved. For degrees less than about 30, the 5° model appears to give an adequate description but for higher degrees the 5° model contains significant power out to high degrees. Thus if the solution (22) of the sea-level equation has not converged by degree $N_{max} \simeq 30$, it will be necessary to adopt the more refined ice grid system.

In both ice models it is assumed that the maximum extent of the ice sheets developed over a sufficiently long time so that the Earth responded sufficiently for an isostatic state to have been achieved by 18 ka BP. This assumption has been questioned by Wu & Peltier (1982) who suggested that the effects of earlier cycles of glaciation and deglaciation may still be seen in some aspects of the Earth's response (see also Peltier 1984). This point is examined further in Section 7.

OCEAN FUNCTIONS

In past studies of the global variations in sea-level, fairly coarse definitions of the ocean functions have been made. Nakiboglu *et al.* (1983) used a 10° resolution; Lambeck &

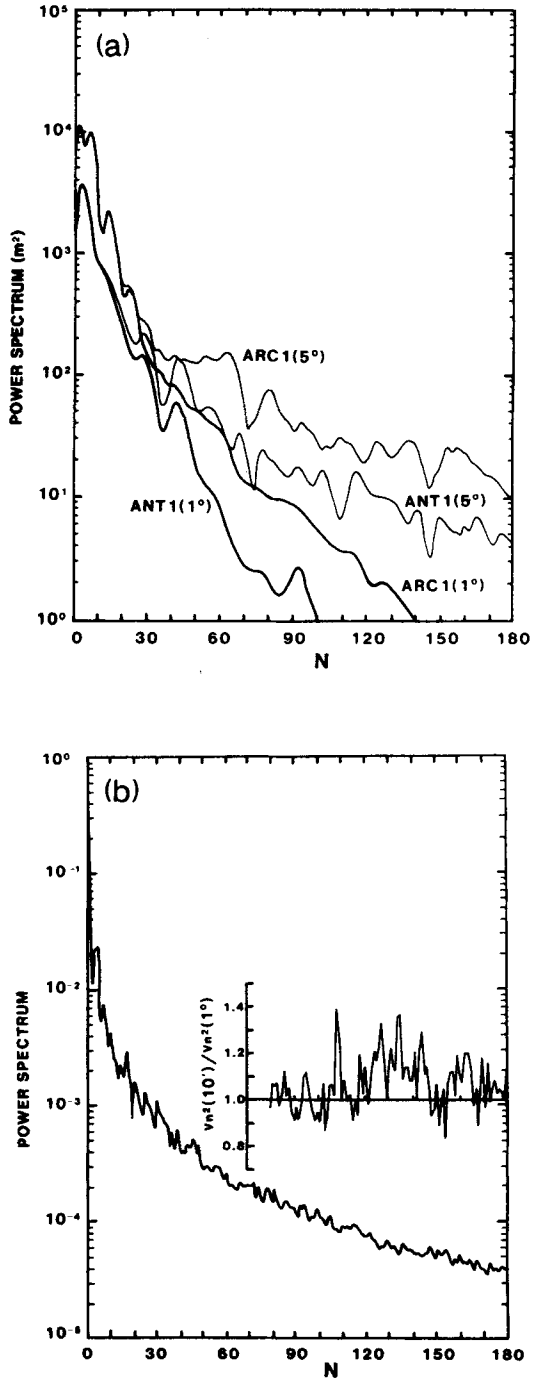

Figure 4. (a) Power spectra of the ARC 1 and ANT 1 ice models based on the 5° and 1° spatial resolutions of the ice load. The spectrum is for the total change in ice load from 18 ka BP to the end of deglaciation. (b) Power spectrum of the ocean function, derived from the dataset with 10′ spatial resolution. The inset illustrates the ratio of the power of two expansions of the ocean function: $V_n^2(10')$ based on the 10′ dataset and $V_n^2(1°)$ based on a dataset with 1° spatial resolution.

Nakada (1985) used 5°, as did Cathles (1975). Wu & Peltier (1983) used a variable resolution; of about 5° in the near-field and along some continental margins and as large as 20° in mid oceans of the far-field. Such models assume that there is no significant differential mantle-flow on these scales and that, within these areas, sea-levels vary through time by the same amount. As discussed in the introduction several observations suggest that variations do occur over relatively short distances. To examine the dependence of the sea-level response on the definition of the ocean function, we use two spatially defined ocean functions, one of 1° resolution the other of 10′ resolution. In the former model, ocean islands such as Tahiti are not defined, and sea-level solutions based on it ignore possible differential movement between the seafloor and the island (Nakada 1986). The two ocean function models may also produce different relative sea-level results at continental margin sites of short-wavelength shoreline geometry such as occur, for example, in the Hauraki Gulf of New Zealand.

The 1° ocean function has been derived from the bathymetry file of Schwiderski (1978), supplemented by some marginal ocean basins that were not included in that compilation. The 10′ ocean function is derived from the global 10′ elevation data published by the US Navy (1985). Both models have been expanded into spherical harmonic series up to degree 180 (equation 27). As for the expansion of the ice function, the coefficients tend to become unreliable at degrees approaching the Nyquist frequency of about 180 for the 1° dataset. Fig. 4(b) illustrates the power spectrum based on the 10′ data set. The spectrum ratio $V_n^2(10')/V_n^2(1°)$, also illustrated in this figure, is generally greater than unity for $n > 80$ (for $n < 80$ this ratio does not depart from unity by more than 10 per cent) reflecting the higher resolution of the coastlines and the inclusion of the ocean islands in the high resolution model.

4 Load Love numbers

The response of the planet to surface loading is defined by the load Love numbers of degree n (k_n and h_n) according to equation (4b) for the elastic planet or to equation (8) for the viscoelastic planet. These parameters have been computed in the Laplace domain using the elastic parameters and density model of Dziewonski & Anderson (1981) (Preliminary Reference Earth Model, or PREM), and for the mantle viscosity models summarized in Fig. 5. High viscosity ($\eta = 10^{25}$ Pa s) viscoelastic lithospheres of thickness H are introduced in

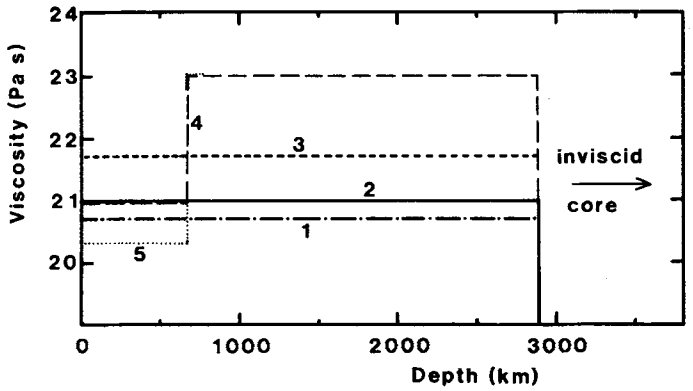

Figure 5. Viscosity models of the Earth. Models 1–3 are for a uniform mantle viscosity. Models 4 and 5 both have a lower mantle viscosity of 10^{23} Pa s.

Table 1. Radial deformation elastic load Love number $(-h_n)$

n	PREM (this study)	1066A(this study)	1066A(Dahlen)
0	0.13433	0.13675	013460
1	0.28969	0.29591	0.29243
2	1.00566	1.02127	1.00959
3	1.06802	1.08764	1.07406
4	1.07241	1.09409	1.07989
5	1.10715	1.13091	1.11606
6	1.16680	1.19305	1.17735
7	1.23764	1.26673	1.25006
8	1.31155	1.34370	1.32602
9	1.38474	1.42010	1.40142
10	1.45570	1.49437	1.47471
11	1.52391	1.56597	1.54538
12	1.58927	1.63480	1.61330
13	1.65180	1.70088	1.67851
14	1.71159	1.76428	1.74106
15	1.76870	1.82506	1.80104
16	1.82321	1.88330	1.85850
17	1.87520	1.93905	1.91350
18	1.92473	1.99237	1.96611
19	1.97188	2.04334	2.01638
20	2.01674	2.09201	2.06439
21	2.05939	2.13845	2.11020
22	2.09991	2.18275	2.15390
23	2.13839	2.22498	2.19555
24	2.17493	2.26523	2.23525
25	2.20962	2.30358	2.27306
26	2.24256	2.34011	2.30909
27	2.27384	2.37491	2.34341
28	2.30354	2.40808	2.37611
29	2.33177	2.43968	2.40727
30	2.35860	2.46981	2.43698
31	2.38412	2.49854	2.46530
32	2.40841	2.52595	2.49233
33	2.43154	2.55212	2.51812
34	2.45358	2.57711	2.54276
35	2.47461	2.60100	2.56630
36	2.49468	2.62385	2.58882

some models. The core is assumed to be inviscid in all models. As a check on these calculations the elastic Love numbers have been evaluated at large values for the Laplace transform variable s and Table 1 summarizes some results for $s = 10^5\ s^{-1}$. The use of larger s values does not change these results. The elastic parameters have also been computed for the elastic earth model 1066A of Gilbert & Dziewonski (1975) to permit a comparison to be made with the results of Dahlen (1976). Agreement is within 1.5 per cent and adequate for all present purposes.

In the time domain the Love numbers for the viscoelastic earth become time-dependent and the consequence of their variation through time on sea-level variations can be best illustrated by the power spectrum of the combination $f_n = [1 + k_n(t) - h_n(t)]$. This spectrum is illustrated in Fig. 6 for several earth models at a time 10 ka after the application of a Heaviside load function. The notation for these models is (j, H) corresponding to the mantle viscosity model j of Fig. 5 and a lithosphere of thickness H (in km). In model (2, 0) (uniform mantle viscosity without a lithosphere) the spectral amplitudes f_n^2 of the Earth's response increases with increasing degree to asymptotic values. If, however, a high-viscosity lithosphere is added, f_n^2 reaches a maximum and then decays at a rate that is a function of the lithospheric thickness and which, at high n, approaches the elastic earth response.

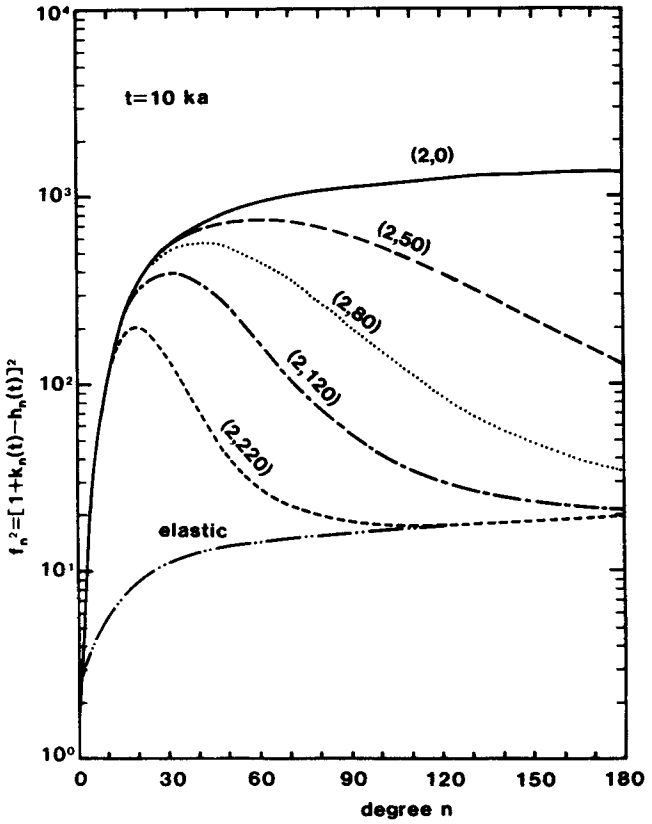

Figure 6. The Earth's response function $[1 + [k_n(t) - h_n(t)]]^2$ for a Heaviside step function load applied at $t = 0$. The response is evaluated at $t = 10$ ka after the time of loading. The mantle viscosity corresponds to model 2 of Fig. 5 with a lithospheric thickness H of 0, 50, 80, 120 and 220 km, respectively. The elastic response is independent of H.

5 Observations of sea-level change

We do not attempt, in this paper, to comprehensively examine sea-levels around the world. Instead, we have selected a few well documented observations to illustrate special aspects of the solution of the sea-level equation, or observations that have played a major role in past discussions of sea-level change. Table 2 and Fig. 7 summarize the selected sites. Sites 1–3 and 10 lie near the centres of the major ice sheets at the time of maximum glaciation. Sites

Table 2. Locations used in this study.

	Name	Co-lat.	E-long.	Figure	Data Source
1	Churchill	31.2	265.8	8	Walcott (1972)
2	Cape Henrietta Maria	34.8	277.7	18a	Walcott (1972)
3	Ottawa Island	30.5	280.0	18b	Walcott (1972)
4	Newfoundland	38.4	304.6	19a	Walcott (1972)
5	Boston	47.7	288.9	19b	Kaye & Barghoorn (1964)
6	Brigantine	50.6	285.6	19c	Walcott (1972)
7	Southport	56.0	282.0	20a	Newman et al. (1980)
8	Miami	64.3	279.8	20b	Walcott (1972)
9	Bermuda	57.7	295.2	20c	Newmann (1971)
10	Angerman River	27.4	17.9	18c	Liden (1938)
11	Karumba	107.3	140.8	21c	Chappell et al. (1982)
12	Hauraki Gulf	126.4	170.0	21b	Gibb (1985)
13	Tahiti	107.5	210.5	21a	Pirazzoli et al. (1985)
14	Tokyo	54.3	139.8	15	Sugimura (1977)

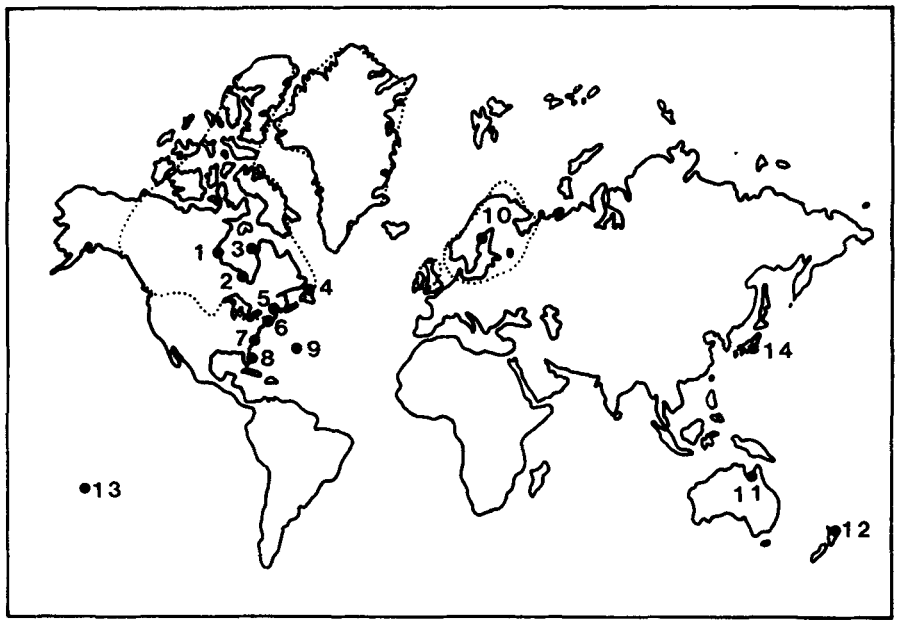

Figure 7. Location map of the late Pleistocene northern hemisphere ice sheets and sites at which relative sea-levels have been evaluated (see Table 2).

4–6 lie near the edge of this maximum ice sheet. Sites 7–9 lie in the near-field at continental margin and island (site 9) locations. Sites 11–14 in the SW Pacific lie in the 'far' field of the Arctic ice sheet and in the 'intermediate' field of the Antarctic ice sheet. The observed quantities are the relative sea-levels at time t, where t_0 is the present time

$$\Delta\zeta(\theta, \lambda: t) = \zeta(\theta, \lambda: t) - \zeta(\theta, \lambda: t_0). \tag{37a}$$

The observations, together with one standard deviation error bars where available, are illustrated in Figs 18–20. References to the data sources are given in Table 1.

6 Convergence of the sea-level equation

To obtain realistic models of the mechanical response of the Earth to a given surface load using the formulation established in Section 2 it is important that both the ice load and the ocean function are defined with an adequate resolution and that the various summations are carried out to a commensurate degree N_{max}. Relative sea-level during the post-glacial phase is defined as

$$\Delta\zeta(\theta, \lambda: t) = \Delta Z_1 + \Delta Z_2, \tag{37b}$$

where

$$\Delta Z_1 = [Z_1(\theta, \lambda: t) - \langle Z_1(\theta, \lambda: t)\rangle] - [Z_1(\theta, \lambda: t_0) - \langle Z_1(\theta, \lambda: t_0)\rangle]$$

$$\Delta Z_2 = [Z_2(\theta, \lambda: t) - \langle Z_2(\theta, \lambda: t)\rangle] - [Z_2(\theta, \lambda: t_0) - \langle Z_2(\theta, \lambda: t_0)\rangle]$$

and the Z_i have been defined by equations (25), (28), (30) and (31). We examine here the requirements for convergence at the time $t = 6.0$ ka BP and the results will be applicable for the entire period of deglaciation as well as for the Holocene

SOLUTIONS WITH 5° ICE MODEL AND 1° OCEAN FUNCTION

Figs 8–10 illustrate the relative sea-levels at 6 ka BP as a function of the maximum degree N_{max} of the summations in equations such as (25). The solutions, at a number of representative sites within the limits of the ice sheets and in the near-field, are based on the 5° ice load models and on the 1° ocean function. Fig. 8 is for the uniform mantle viscosity of $\eta = 5 \times 10^{20}$ Pa s model (1, 0) without a lithosphere. The relative sea-levels have generally converged adequately by degree $N_{max} \simeq 90$ except at the sites of Boston and Brigantine which both lie near the edge of the former ice sheet. At these sites higher N_{max} are necessary if a precision of a few metres is required. Convergence is more rapid if the viscosity is increased, as is illustrated in Figs 9 and 10 for models (2, 0) ($\eta = 10^{21}$ Pa s) and (3, 0) ($\eta = 5 \times 10^{21}$ Pa s), and, for the latter, satisfactory convergence is reached by $N_{max} \simeq 36$ at most sites and by $N_{max} \simeq 90$ at Boston and Brigantine.

In the far-field the changes in Holocene relative sea-level fluctuations are smaller than in the near-field but in many instances the Holocene high stands can be defined with considerable precision. At some far-field sites convergence is relatively slow for low viscosity models (1, 0) (Fig. 11); at the Hauraki Gulf, near Auckland (New Zealand), for example, convergence may not have been reached with $N_{max} \simeq 180$ (Fig. 11a). The Antarctic contribution also converges slowly at the latter site (Fig. 11b). For models with higher mantle viscosity (3, 0), convergence at all these sites is achieved by $N_{max} \simeq 40$ (Fig. 12).

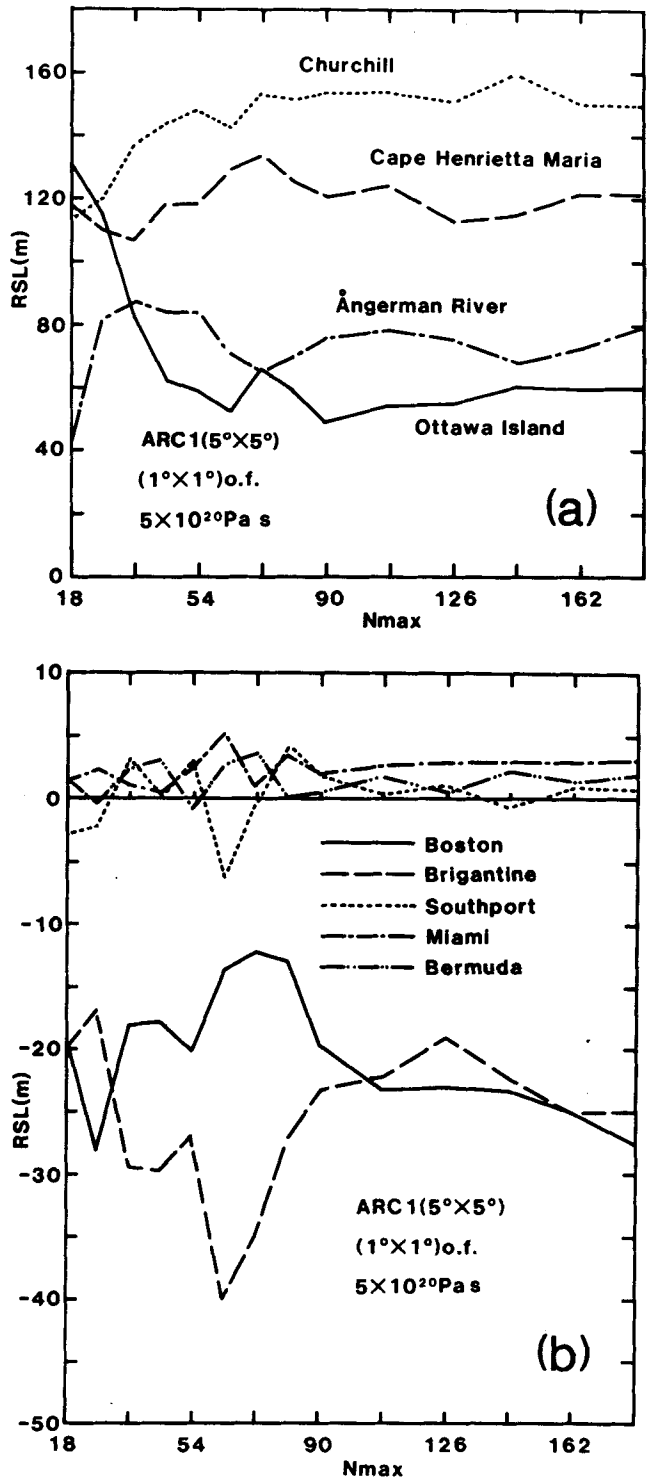

Figure 8. Relative sea-levels at 6 ka BP at sites within the limits of the former ice sheet (a) and near the edge of the load (b) as a function of the degree N_{max} of truncation of the solution of the sea-level equation for Earth model 1 without lithosphere.

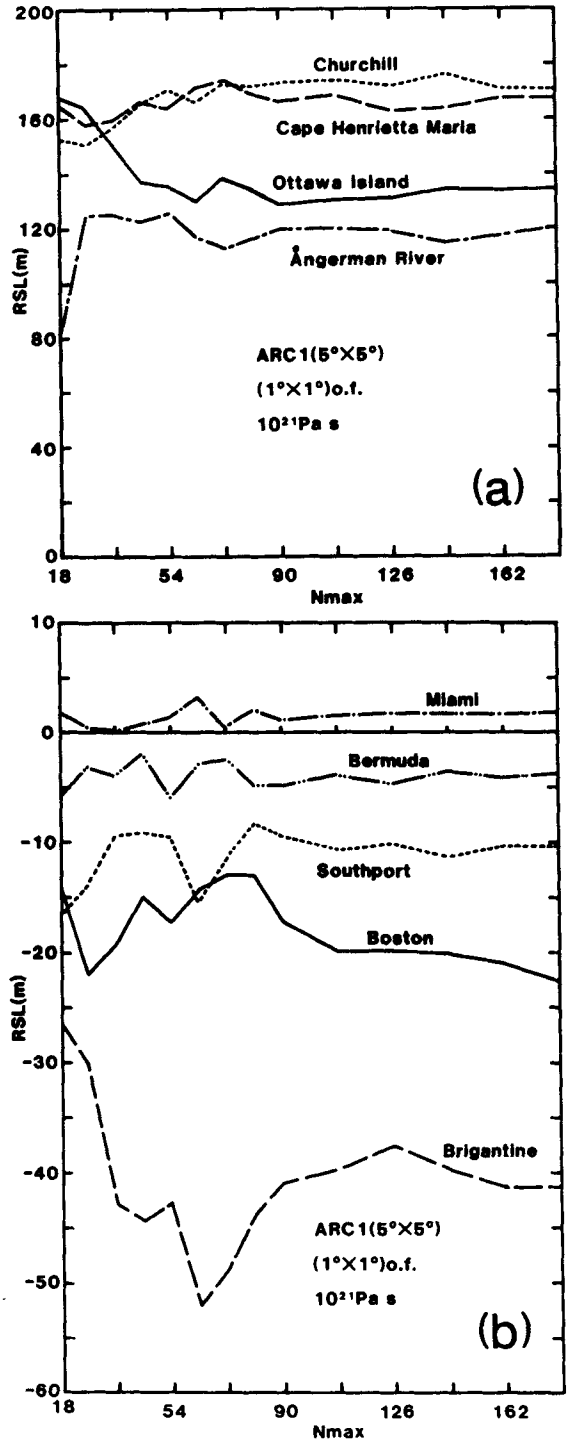

Figure 9. Same as Fig. 8 but for mantle model 2 without lithosphere.

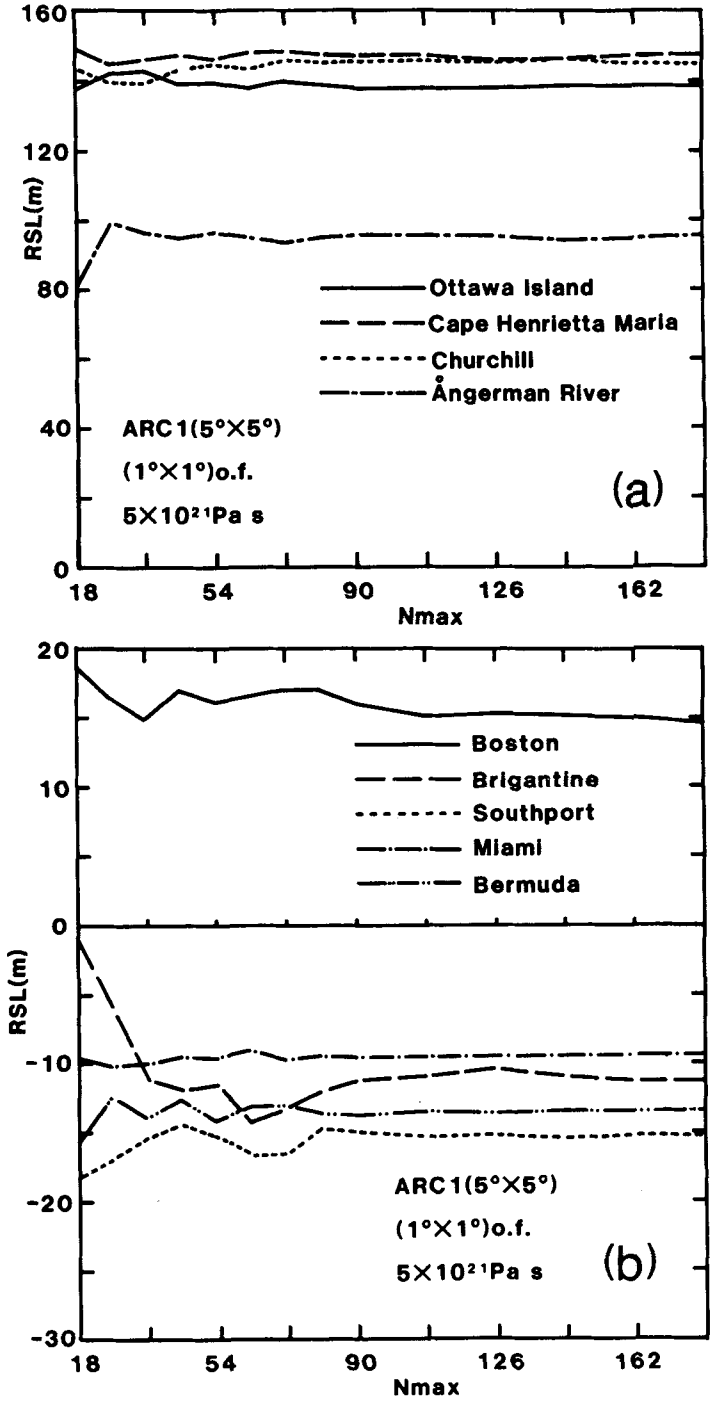

Figure 10. Same as Fig. 8 but for mantle model 3 without lithosphere.

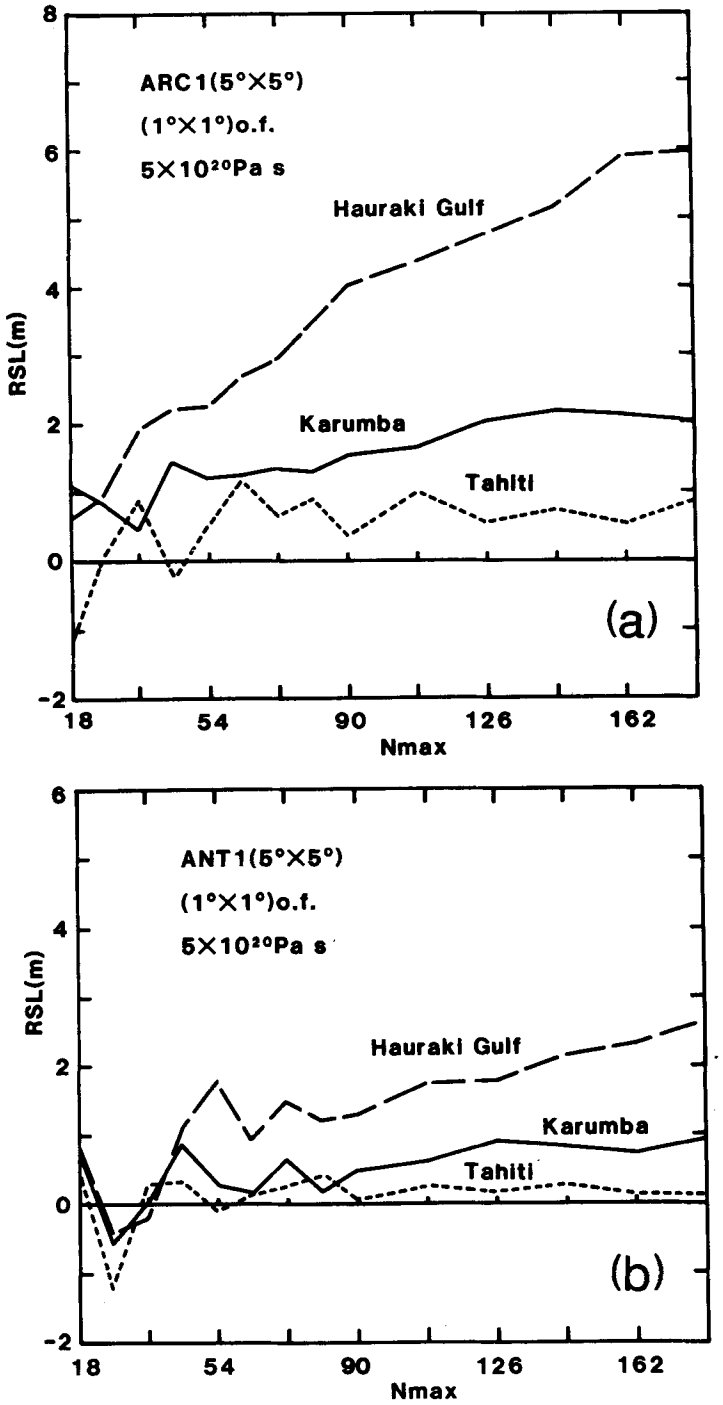

Figure 11. Relative sea-levels in the far-field at 6 ka BP as a function of the degree of truncation of the solution of the sea-level equation for mantle model 1 without lithosphere: (a) is for the Arctic ice model ARC 1 and (b) is for the Antarctic melting model ANT 1.

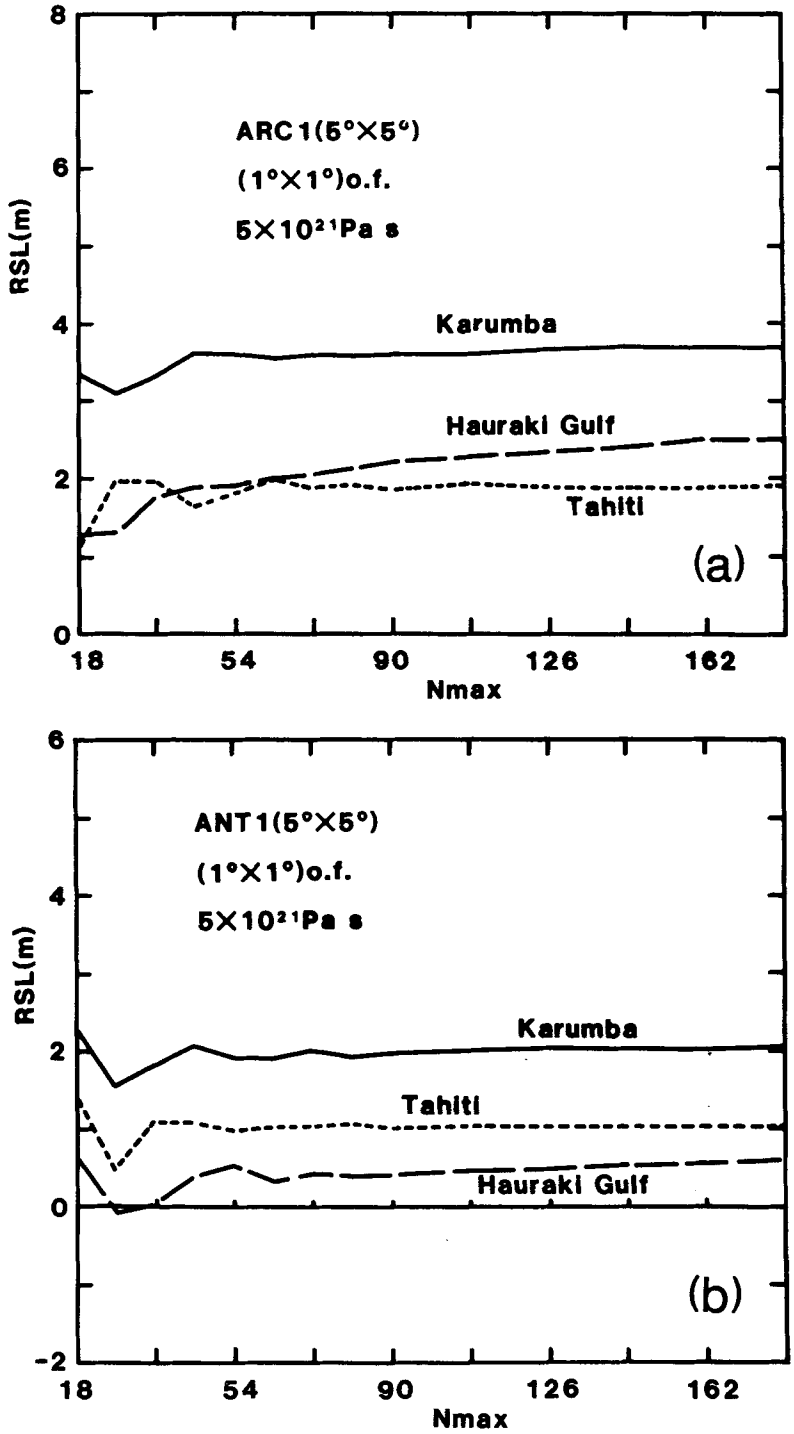

Figure 12. Same as Fig. 11 but for model 3 without lithosphere.

Figs 8–12, and similar results at other sites for Earth models without lithospheres, illustrate several points:

(i) An increase in effective mantle viscosity results in improved convergence of the summations in the relative sea-level equation (37).

(ii) The convergence at sites within the Hudson Bay, at the centre of the late Pleistocene sheet, remains relatively stable for the three rheological models provided that $N_{max} \gtrsim 54$.

(iii) The relative sea-levels at the edge of the ice sheet, such as the sites of Boston and Brigantine, are very unstable.

(iv) The relative sea-levels along continental margins and at small ocean islands for the far-field are relatively stable for $N_{max} \gtrsim 54$, although at some sites, such as those in New Zealand, the Holocene maximum increases with increasing N_{max}.

The first observation is a consequence of the higher degree deformation reflecting mainly the response of the upper mantle and as the mantle viscosity is increased these high-degree contributions to the sea-level change decrease. The second observation is a consequence of sea-levels at these sites reflecting predominantly the lower degree deformation because of the large wavelength of the ice load. At low N_{max} the convergence behaviour at Ottawa Island is distinctly different from that at Churchill and Cape Henrietta Maria (compare Figs 8 and 9) because these latter two sites are located closer to the central part of the former ice sheet. The explanation of observation (iii) is that the sea-level change at sites near the edge of the ice sheet is sensitive to the short wavelength deformations characterizing the expansion of the step-like ice function at the margins. The fourth observation, of increasing Holocene highs with increasing degree is directly associated with the local isostatic adjustment to the added meltwater (see also Nakada 1986) and this is discussed further below.

These calculations demonstrate that solutions for the sea-level equation based on the 5° ice models and with $N_{max} = 36$ are inadequate; for many locations the series expansions will not have converged unless the effective mantle viscosity is equal to, or exceeds about 5×10^{21} or 10^{21} Pa s, Solutions with a greater N_{max} will generally be required but this demands higher resolution expansions of the ice model.

SOLUTIONS WITH 1° ICE MODELS AND 1° OCEAN FUNCTION

To examine the convergence behaviour in greater detail the 1° linearly interpolated ice model is used and the terms ΔZ_1 and ΔZ_2 in the relative sea-level equation (37) are evaluated separately. Fig. 13 illustrates ΔZ_1 at 6 ka BP for two sites located near the centre of maximum loading. This term represents the contribution to relative sea-level arising from the glacial unloading of the crust and at these sites, as well as at sites in the near-field, it is the dominant term in the sea-level equation. The results are illustrated for viscosity models (1, 0) and (2, 0) and for both the 1° and 5° representations of the ARC 1 ice model. The convergence behaviour of the 1° solution is considerably better than that of the 5° solution and this is also well illustrated by the results at the edge of the ice sheet (Fig. 14). In general, satisfactory convergence at near-field sites is achieved with $N_{max} \approx 90$. This means that any uncertainties in the higher degree terms ($90 < n < 180$) resulting from the spherical harmonic expansions are unimportant and there is no need to establish a finer grid for the ice model.

The far-field solutions for the Arctic ice model ARC 1 are illustrated in Fig. 15. Here the ΔZ_2 term, due to the loading of the ocean by the meltwater, is generally of greater importance than the ice load term ΔZ_1. At all sites examined, the convergence of ΔZ_1 with increasing N_{max} is rapid if the 1° ice models are adopted. The ΔZ_2 term at these sites is identical for both representations of the ice models. This is a consequence of the excitation function $F_n(t)$ in equation (21) so that this term is proportional to the volume of the melt-

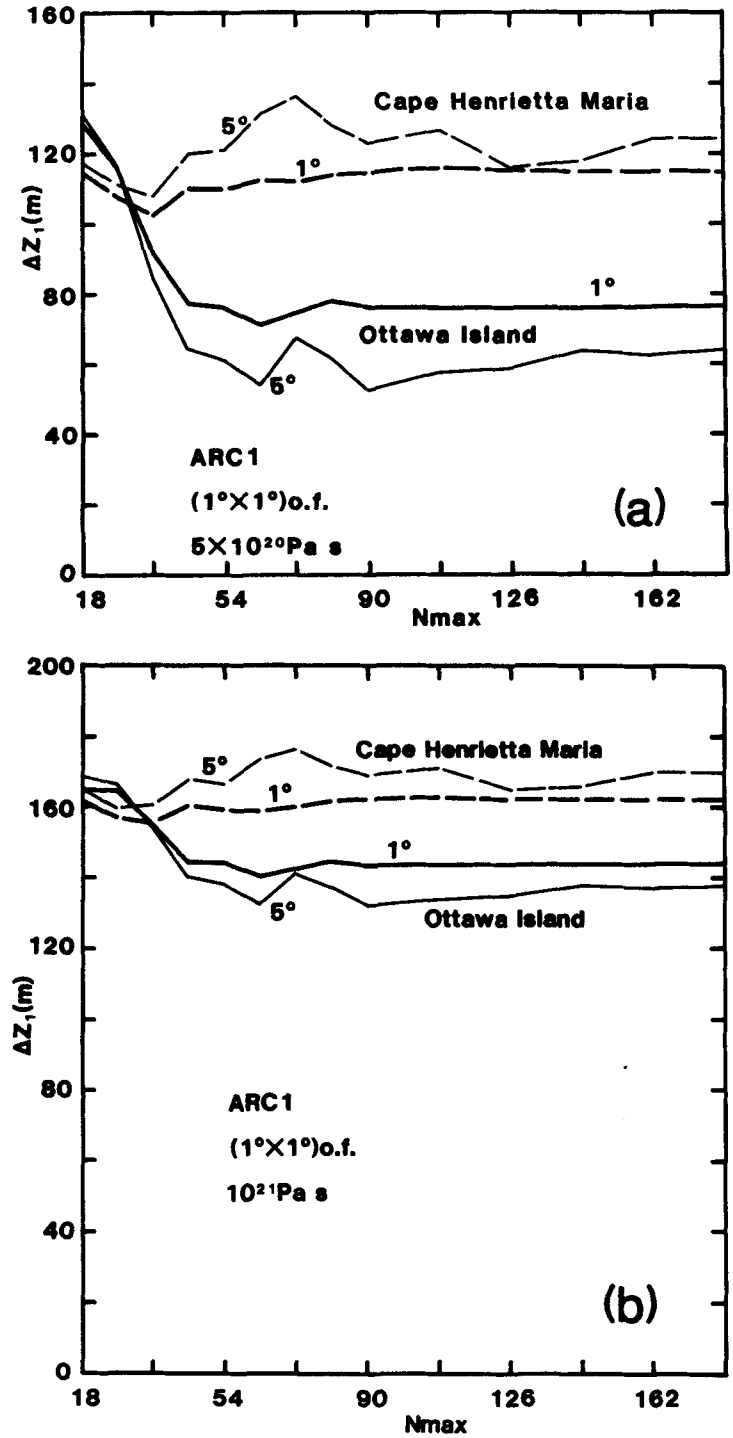

Figure 13. Contribution to relative sea-level at 6 ka BP from the term ΔZ_i of equation (37b), representing the response to unloading of the ice. Two representations of the ice model are used; the 5° ice model and the linearly interpolated 1° model: (a) is for mantle model 1 and (b) is for mantle model 2, both without lithosphere. Both sites lie within the interior of the former ice sheets.

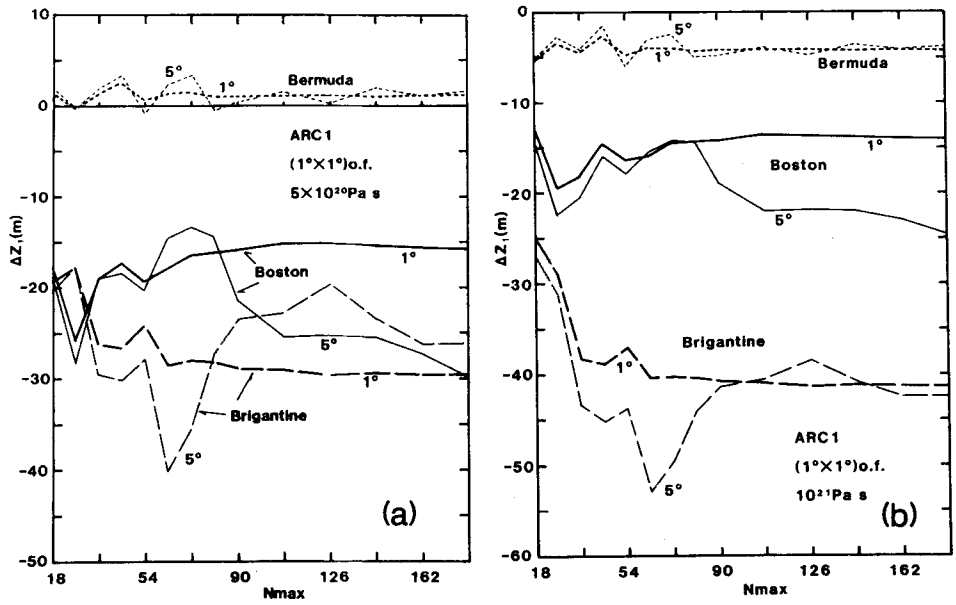

Figure 14. Same as Fig. 13 but for sites near the edge of the former ice sheet.

water. The contribution of ΔZ_2 to sea-level change from the Antarctic deglaciation (Figs 15d–f) is about one-half of that from the Arctic, as would be anticipated from their relative contributions to the total meltwater added to the oceans (see Fig. 3). The ΔZ_2 term is the dominant contribution to relative sea-level at the site of the Hauraki Gulf in New Zealand and here ΔZ_2 has not converged even by $N_{max} = 180$. Similar results have been found for other locations on large islands, such as Japan (see Fig. 15b) and New Guinea.

The major conclusions that can be drawn from Figs 13–15 are:

(i) The use of a high-resolution ice model leads to a more satisfactory convergence of the relative sea-levels at sites in the near-field, particularly for sites near the edge of the ice load.

(ii) In the far-field the dominant contribution to the Holocene sea-level change comes from the response of the crust to the water load.

(iii) The ΔZ_2 term does not converge at all sites in the far field; particularly at sites where the coastline geometry is complex.

The first observation is the result of the reduced power of the smoothed ice function at high degrees (Fig. 4a). The third observation is associated with an inadequate definition of the ocean function at these sites. From equations (21) and (22) and the definitions of the functions Q_n and F_n, the term Z_2 is a consequence of the added meltwater and the mantle flow in response to this load from the ocean side to the island side. It appears that a greater resolution for the ocean function is required at some sites in order to adequately model this effect.

For sites where large N_{max} are required to produce converged solutions, it is important that the spherical harmonic coefficients of the ocean function are precisely computed. Fig. 4(b) illustrates that this is not the case if these coefficients are based on $1^\circ \times 1^\circ$ area means of the ocean function; the expansion based on the $10' \times 10'$ area means produces some significant differences for degrees greater than about 100 and the question may well be asked, therefore, is whether this lack of convergence is a consequence of the inadequacy of the ocean function used to produce the results illustrated in Figs 8–15. A comparison of the

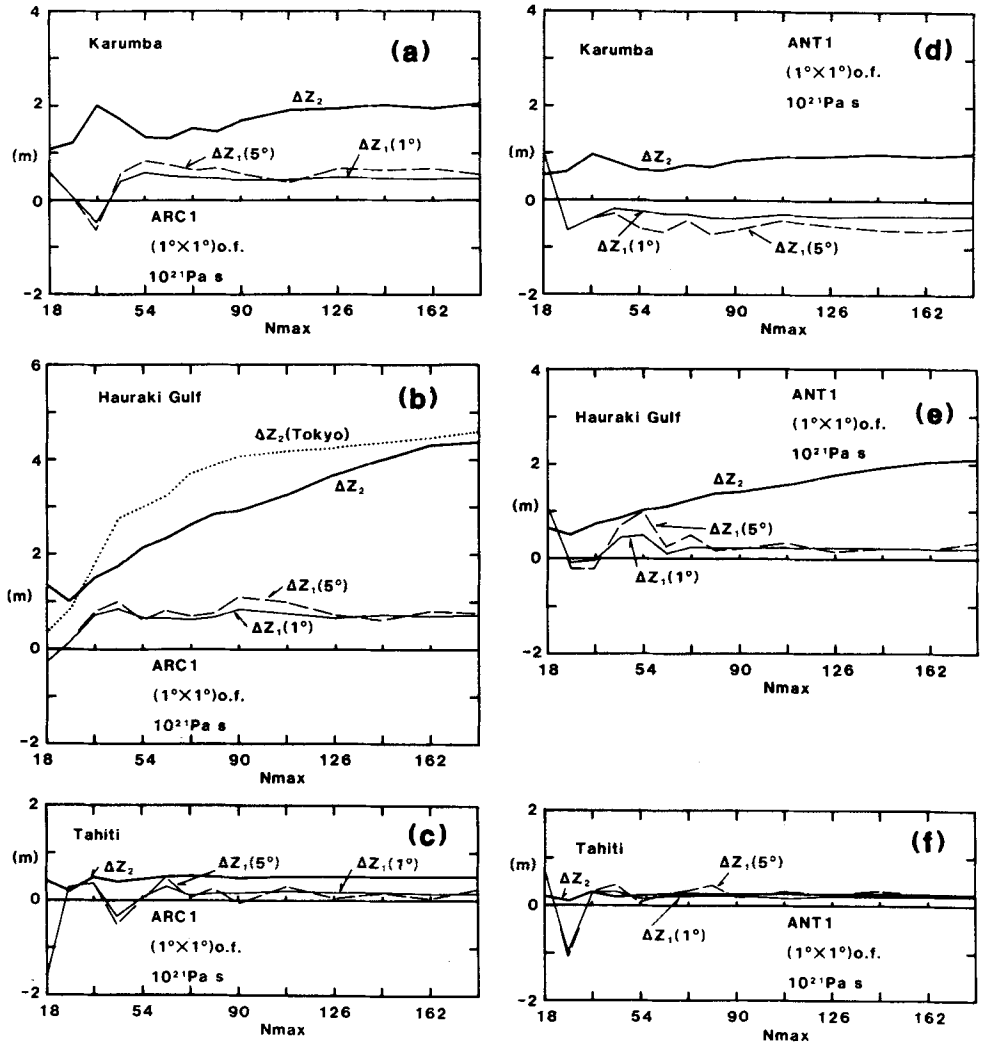

Figure 15. Same as Fig. 13 but for sites in the far-field. Both the contributions ΔZ_1 and ΔZ_2 are illustrated with the latter term representing the response to the added meltwater. The results on the left are for the Arctic ice model ARC 1 and the results on the right are for the Antarctic ice model ANT 1.

two expansions in the spatial domain indicates that islands such as Tahiti are not resolved in the degree 180 expansion based on the 1° database and in this case the sea-level response is simply that of the open seafloor upon which the meltwater is uniformly distributed. Convergence of the solution can therefore be expected to be quite rapid (Fig. 16a). For the 10′ data set the expansion up to degree 180 partly resolves the island and the differential loading of the crust is partly modelled, with the consequence that mantle flow occurs from beneath the oceanic crust to beneath the island or vice versa. The expansion to $N_{max} = 180$ is inadequate to resolve this relative deformation and the solution for relative sea-level does not converge (Fig. 16a). The appropriate solution for this geometry is essentially one of estimating the deflection of a viscous or viscoelastic medium at the point of application of a delta-function load (in space). To achieve convergence, an even higher N_{max} is required (see

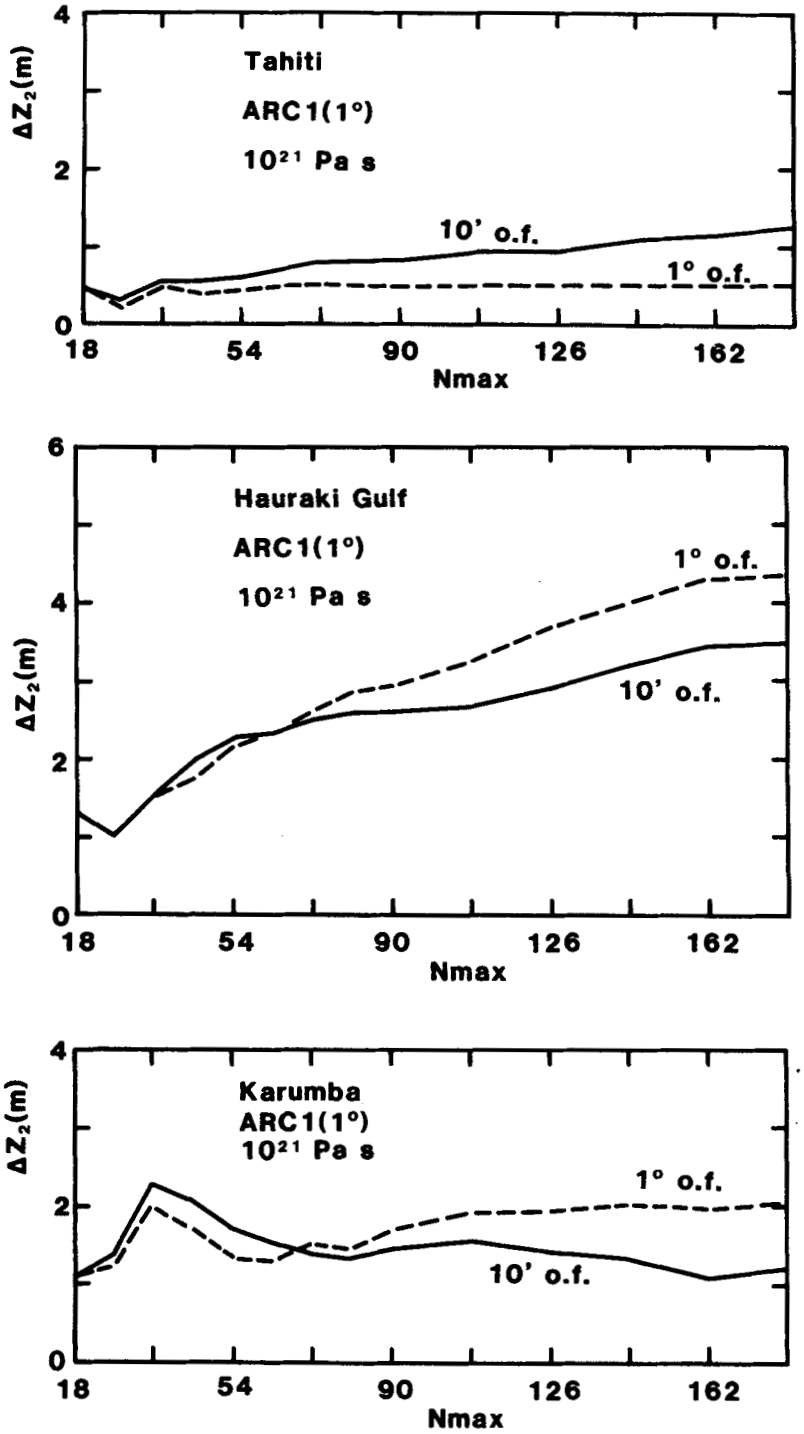

Figure 16. Relative sea-levels at 6 ka BP in the far-field as a function of the degree of truncation for the 1° and 10′ representations of the ocean function. The Earth model is the viscosity structure 2 without lithosphere.

Appendix) unless the solution is stabilized by either increasing the mantle viscosity or by introducing a thick-elastic or high-viscosity lithosphere (see below).

At the sites of the Hauraki Gulf and Karumba the 1° description of the ocean function does partly resolve the coastline geometry and mantle flow back and forth from beneath the oceans to beneath the continents is modelled to a degree. The use of the 10′ area means improves the description of this flow but, at least at Hauraki Gulf where the coastline geometry is complex, the convergence is still not satisfactory (Fig. 16b). Here also, an expansion beyond $N_{max} = 180$ appears to be required or the solution needs to be stabilized by some other means.

EARTH MODELS INCLUDING A LITHOSPHERE

The earth models examined so far are geophysically unrealistic in that they do not consider the effects of a strong lithosphere on relative sea-level changes. The strength of the lithosphere is characterized by its effective flexural rigidity

$$D = EH^3/12(1 - \nu^2),$$

where H is the thickness of the layer, E is Young's modulus and ν is Poisson's ratio. All quantities are equivalent or effective parameters. The wavelength λ_r of the regional rebound of this layer, in response to a surface lead, is given approximately by

$$\lambda_r = 4(D/\rho_m g)^{1/4},$$

where ρ_m is the mantle density. If the wavelength of the load is of this order or less, the lithosphere will significantly modify the viscous mantle response. This can be seen immediately from Fig. 6 where the power spectrum of the Earth's response function is considerably damped when the lithospheric thickness is increased: relative sea-level on an earth with a thick lithosphere will have less high-frequency spatial variability than on an earth without a lithosphere. The presence of the lithosphere will therefore have a stabilizing influence on the convergence of the sea-level solution and its introduction can be used to eliminate the need for very high-degree expansions of the ocean function. In this case, however, it cannot be argued that the thick lithosphere has any physical meaning.

We consider models of a lithosphere with E and ν given by PREM. The layer is assumed to have a viscosity of 10^{25} Pa s, high enough for it to behave essentially as an elastic medium on loading time scales of about 10^5 yr. Fig. 17(a) illustrates the consequence of introducing such a lithosphere (of thickness H) on the sea-levels at the sites of Boston and Brigantine, using the 1° ice load and the 10′ ocean function models. Clearly, the thicker the lithosphere the more rapid in the convergence of the sea-level equation. For example, if the expansions are only carried out to degree 36 a lithosphere of about 220 km thickness must be introduced in order to obtain convergence. The introduction of the thick lithosphere also results in an improved convergence if the 5° ice load model is used (compare Fig. 17a with Fig. 9b).

At far-field sites the introduction of a thick lithosphere ensures rapid convergence because of the improved behaviour of the ΔZ_2 term. Fig. 17(c) illustrates this at 6 ka BP for Tahiti where convergence is reached at $N_{max} \simeq 60$ for lithospheric thickness H of 80 km, and at $N_{max} \simeq 36$ for $H = 220$ km. Convergence is also achieved for the Hauraki Gulf and Karumba sites (Fig. 17b, d) at $N_{max} \simeq 180$ for $H = 50$ km, and at $N_{max} \simeq 36$ for $H = 220$ km. At the first site the converged value is sensitive to the choice of H but at the second site the amplitude of relative sea-level at 6 ka BP is quite insensitive to H.

If thick lithospheres are introduced, is the 1° ice function necessary or is the 5°

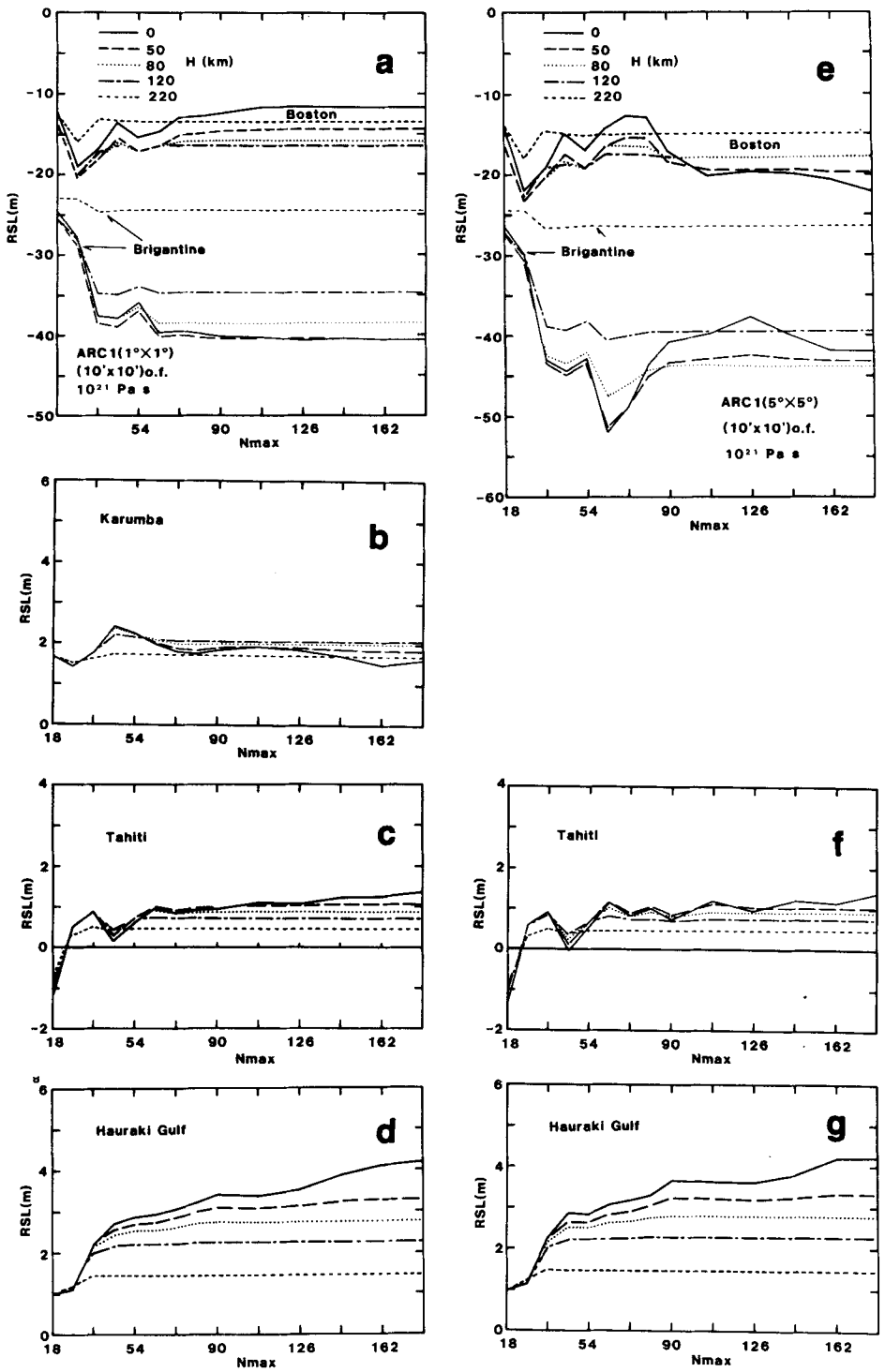

Figure 17. Relative sea-level at 6 ka BP for Earth model 2 with a lithosphere of thickness H (H= 0, 50, 80, 120 and 220 km). The figures on the left are based on the 1° ice model (ARC 1) while those on the right are based on the 5° representation of this ice model. The Karumba results are indistinguishable for the two ice models.

description, as used by most previous investigators, adequate? Fig. 17(e–g) illustrates the predicted sea-levels (at 6 ka BP) based on the 5° ice model and the 10′ ocean function for the viscosity model 2 with a variable-thickness lithosphere. For the 220 km thick layer, convergence is reached by $N_{max} \simeq 36$ at sites near the edge of the ice sheet although the solution does not converge on quite the same value as does the 1° ice solution (compare Fig.

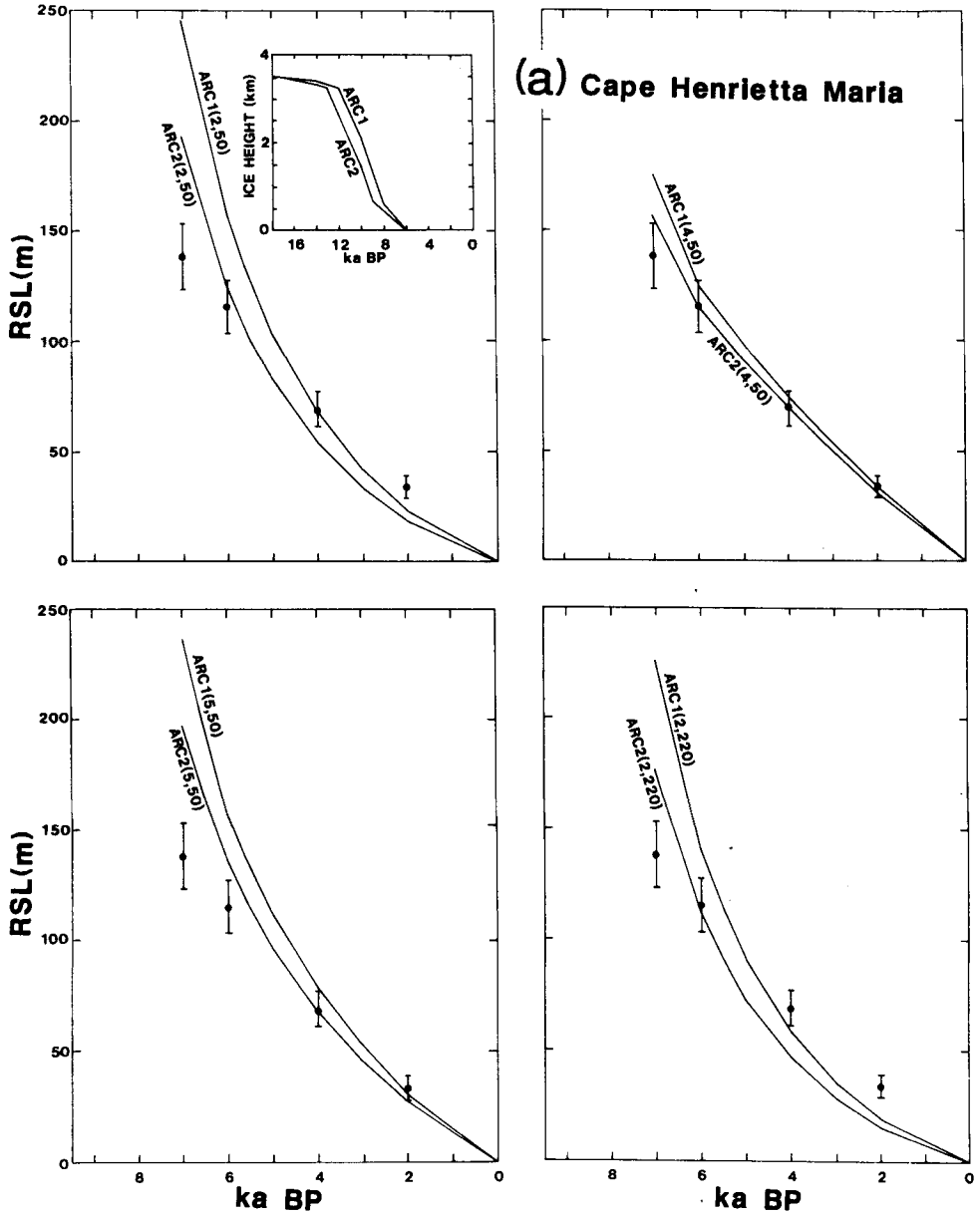

Figure 18. Relative sea-levels at sites near the centres of the Laurentide and Fennoscandian ice sheets (see Fig. 7 for locations) as a function of the ice load, mantle viscosity and lithospheric thickness. Observed sea-levels are indicated by solid circles and $\pm 1\sigma$ error bars (where available). Data sources are listed in Table 2. Insets illustrate the ARC 1, 2 melting histories at these sites. (a) is for Cape Henrietta Mari, (b) is for Ottawa Island and (c) is for Angerman River. For (b) and (c) see pp. 214–215.

17a with 17e, for example) because of difference in detail of the ice distribution near the site. In the far-field the 5° and 1° ice models give very similar results, as would be expected because it is the water load that controls the Holocene sea-level change, the ΔZ_2 term.

SUMMARY OF THE CONVERGENCE REQUIREMENTS

(i) The ice models described by the 5° area means are generally inadequate for evaluating relative sea-levels in the near-field because their spectra contain significant power at high

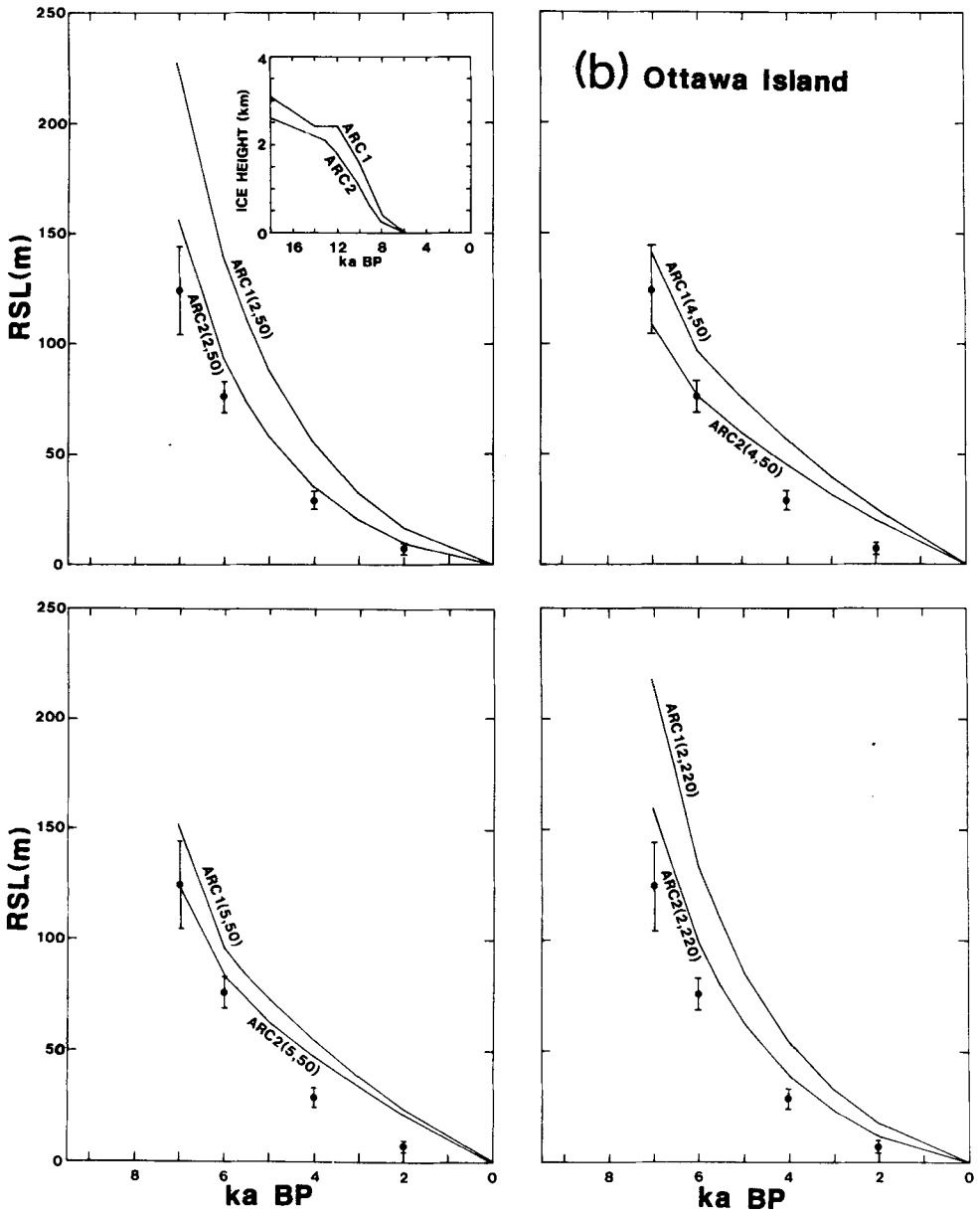

Figure 18 – *continued*

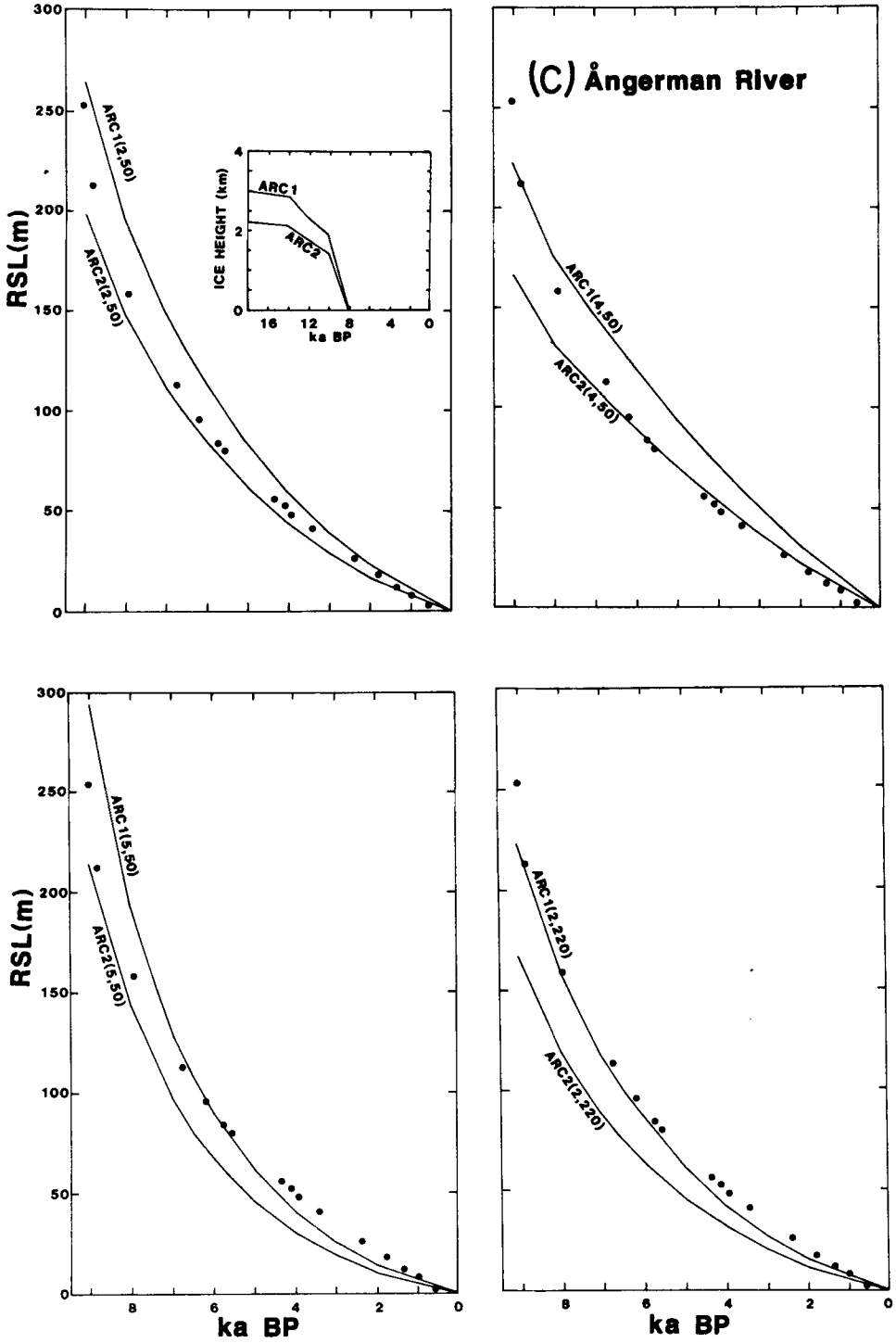

Figure 18 – *continued*

frequencies that is associated with the edge effects of the ice columns. The smoothed ice models with spatial resolution of 1° produce mathematically satisfactory solutions for relative sea-level change at all locations.

(ii) High resolution of the coastline geometry is necessary, and at some sites the expansion needs to be carried out to a high degree ($N_{max} \gtrsim 100$, and in the example of the Hauraki Gulf, $N_{max} \simeq 180$). To obtain an accurate ocean function expansion out to this degree, the required spatial definition of the function is of the order of 10′. The need for a

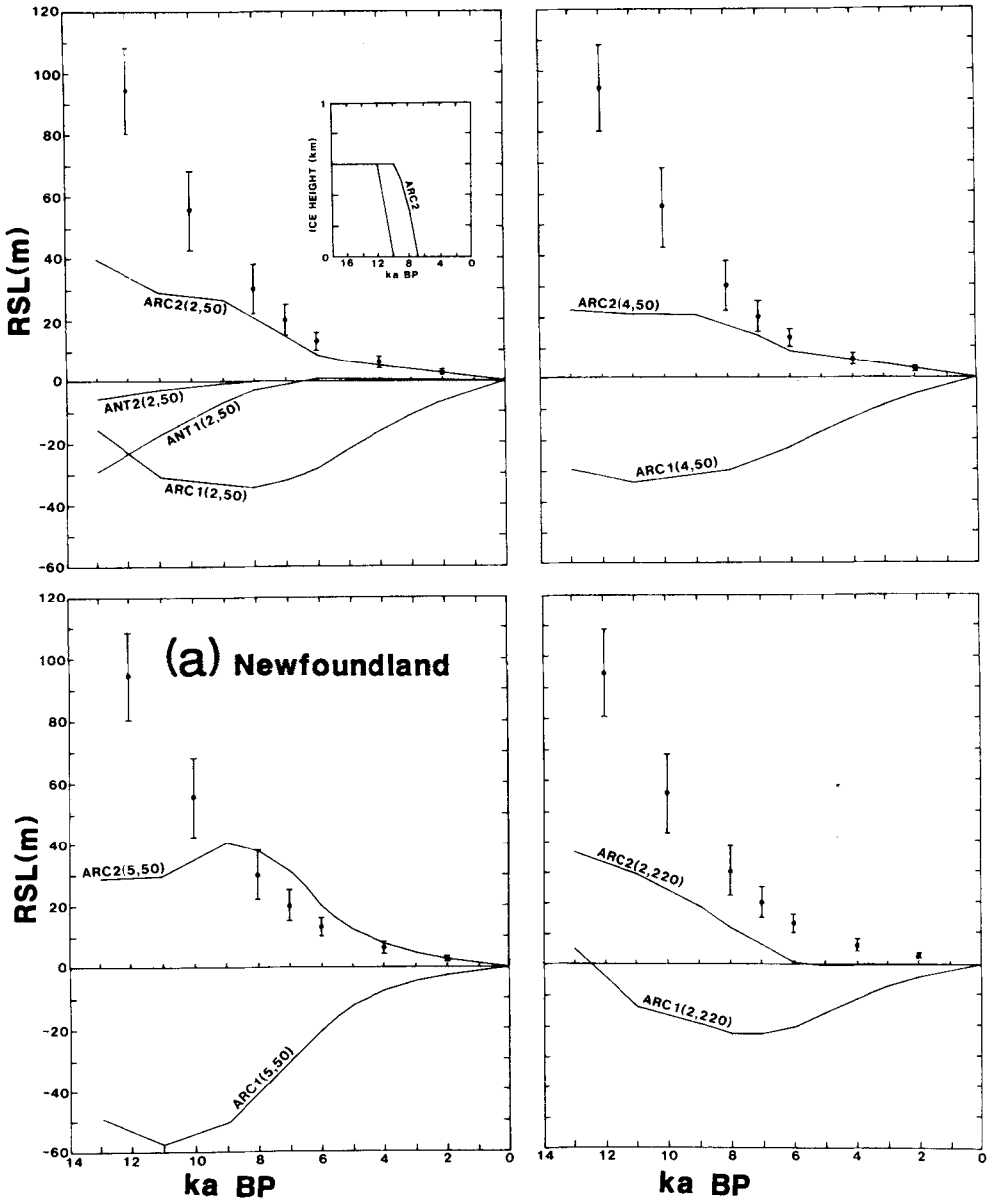

Figure 19. Same as Fig. 18 but for sites near the edge of the Laurentide ice sheet. (a) Newfoundland, (b) Boston, (c) Brigantine. Insets illustrate the melting histories according to models ARC 1 and ARC 2. For Brigantine this corresponds to the nearest ice column.

precise description of the ocean function is particularly important when Holocene sea-levels are examined at island sites in the far-field.

(iii) If lower resolutions for the ice and ocean functions are used then mathematically satisfactory solutions can be obtained by increasing either the mantle viscosity or by introducing thick lithosphere models. For example, the 5° ice sheet produces mathematically satisfactory results in the near-field of $H \simeq 200$ km. In such cases, however, the sea-level data cannot be used to support arguments for a mechanically strong lithosphere.

7 Sensitivity of relative sea-level variations to the deglaciation history and mantle structure

Relative sea-level variations can, depending on their geographical location and time, be quite sensitive to the choice of deglaciation model; to the total volume of meltwater, to the geographical distribution of the ice, and to the rates of melting. Furthermore, the sea-levels are equally or more sensitive to the Earth structure; to the mantle viscosity and to the lithospheric thickness. Figs 18–21 illustrate some of these dependencies for sites near the centres

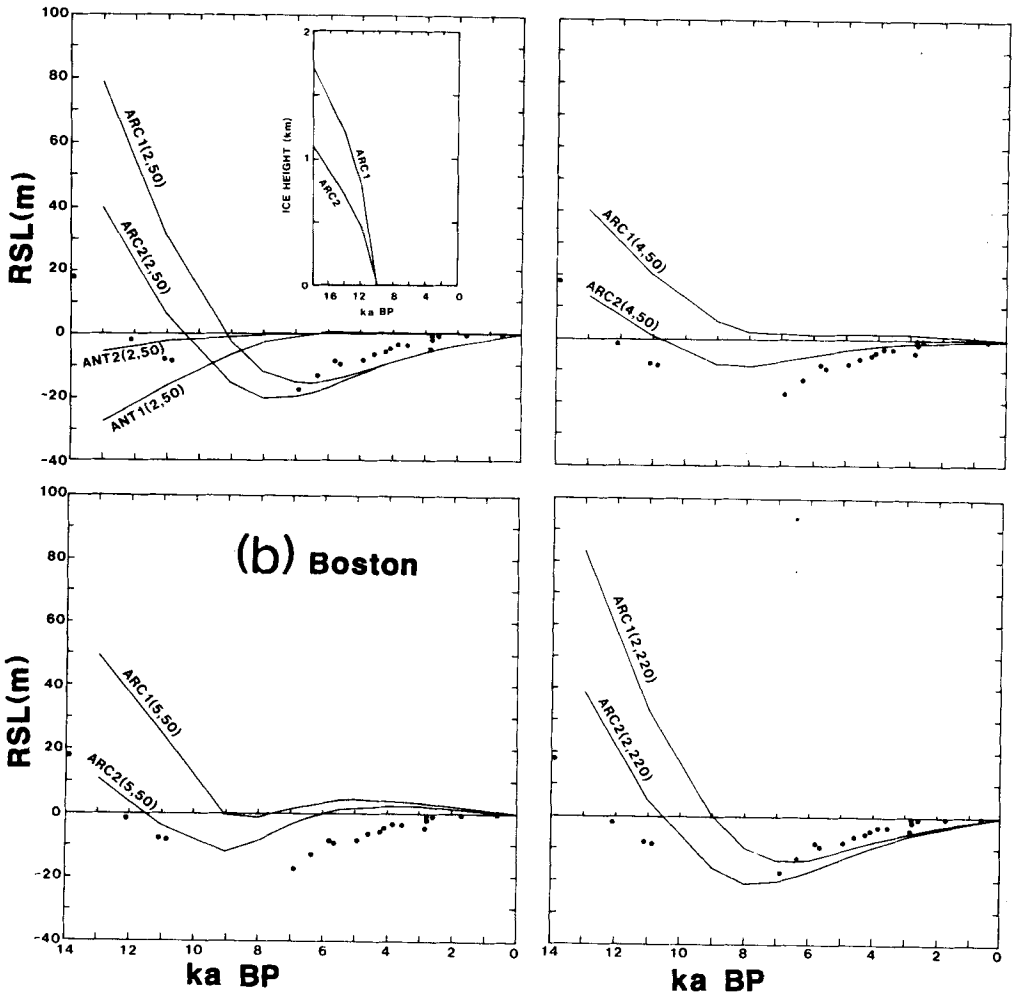

Figure 19 – *continued*

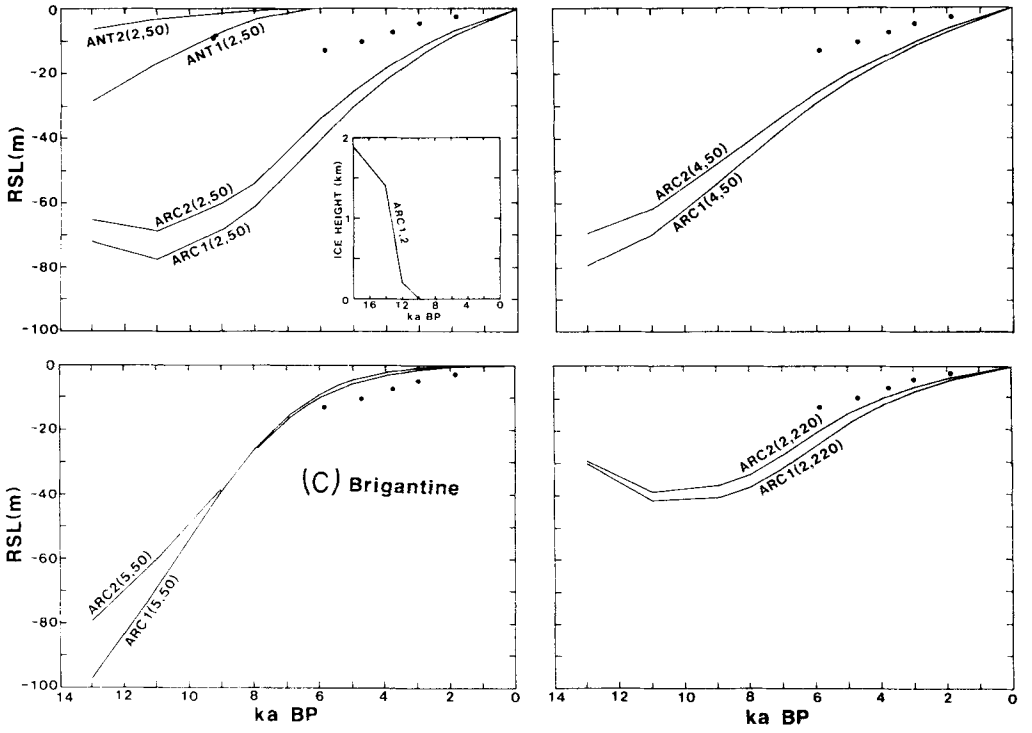

Figure 19 – *continued*

of the former Laurentide and Fennoscandian ice sheets (Fig. 18), for sites near the edge of the Laurentide ice sheet (Fig. 19) and for sites in the near- and far-fields of this ice sheet (Figs 20 and 21, respectively). The notation for the relative sea-level results is of the form ARC $i(j, H)$, where i refers to the Arctic model (ARC 1 or ARC 2), j refers to the mantle viscosity model of Fig. 5, and H refers to the lithospheric thickness. The Earth response model (2, 50) is a nominal one with uniform mantle viscosity of 10^{21} Pa s overlain by a 50 km thick lithosphere. In model (2, 220) this lithospheric thickness has been increased to 220 km, as favoured by Peltier (1984). In model (4, 50) the viscosity of the lower mantle (below 670 km) has been increased to 10^{23} Pa s and model (5, 50) corresponds to an upper mantle with a viscosity of 2×10^{20} Pa s and a lower mantle viscosity of 10^{23} Pa s. These four models cover the range of mantle viscosities that have been proposed in recent years. Also illustrated in these figures are the observed sea-levels during the late stages of deglaciation and during the Holocene. All predicted sea-levels are based on the 1° representation of the ice model and on the ocean function derived from the 10′ resolution dataset. All expansions have been carried out to degree $N_{max} = 180$.

Well within the limits of the former ice sheets, the contributions from Antarctica are relatively small and can be safely ignored. The differences in relative sea-levels predicted by the two Arctic ice models at these sites are typically about 30 per cent, not very dependent on the choice of Earth model, and of a similar magnitude as the uncertainties in the sea-level observations. The ARC 1 load generally leads to an overestimation of the sea-level heights during the late phase of deglaciation and Holocene times and the ARC 2 model gives a better overall agreement with observations; as it should, because it was adjusted, assuming a mantle

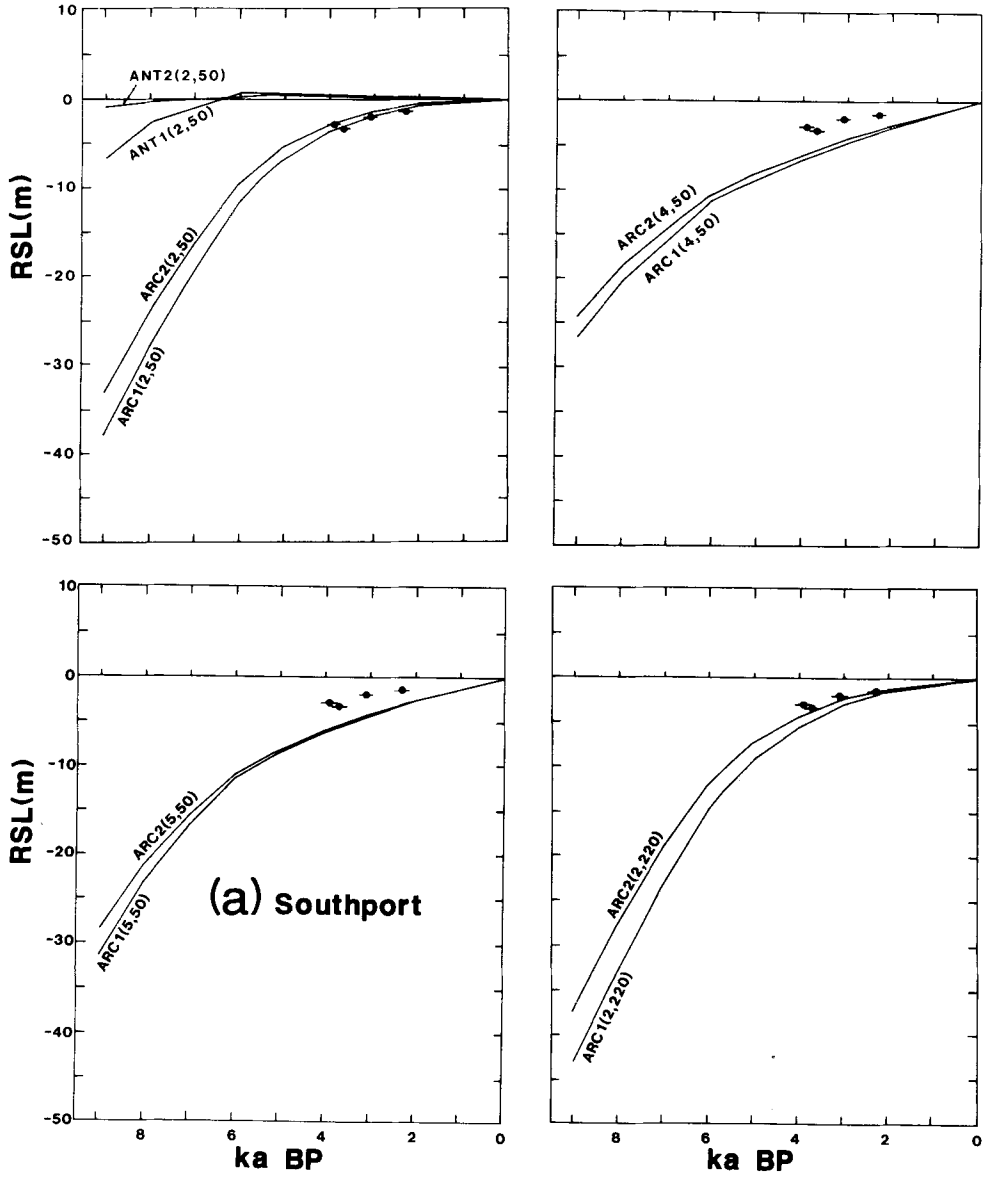

Figure 20. Same as Fig. 18 but for sites in the intermediate field. (a) Southport, (b) Miami, (c) Bermuda.

viscosity of 10^{21} Pa s, to produce sea-levels in the near-field that matched the observations. The dependence of the sea-level variation on mantle viscosity is also not very great and these observations alone do not permit the two sets of model parameters to be separated. Models (2, 50) and (2, 220) predict similar results for locations near the centre of the Laurentide ice sheet, indicating that the response at these sites is not a sensitive indicator of lithospheric thickness H. The Ångermann River site, near the centre of the Fennoscandia ice mass, is more sensitive to H, in keeping with the smaller dimensions of this ice sheet.

Sea-levels near the edge of the former Laurentide ice sheet are sensitive to the choice of ice load and mantle structure because the nearby load contains considerable shorter wave-

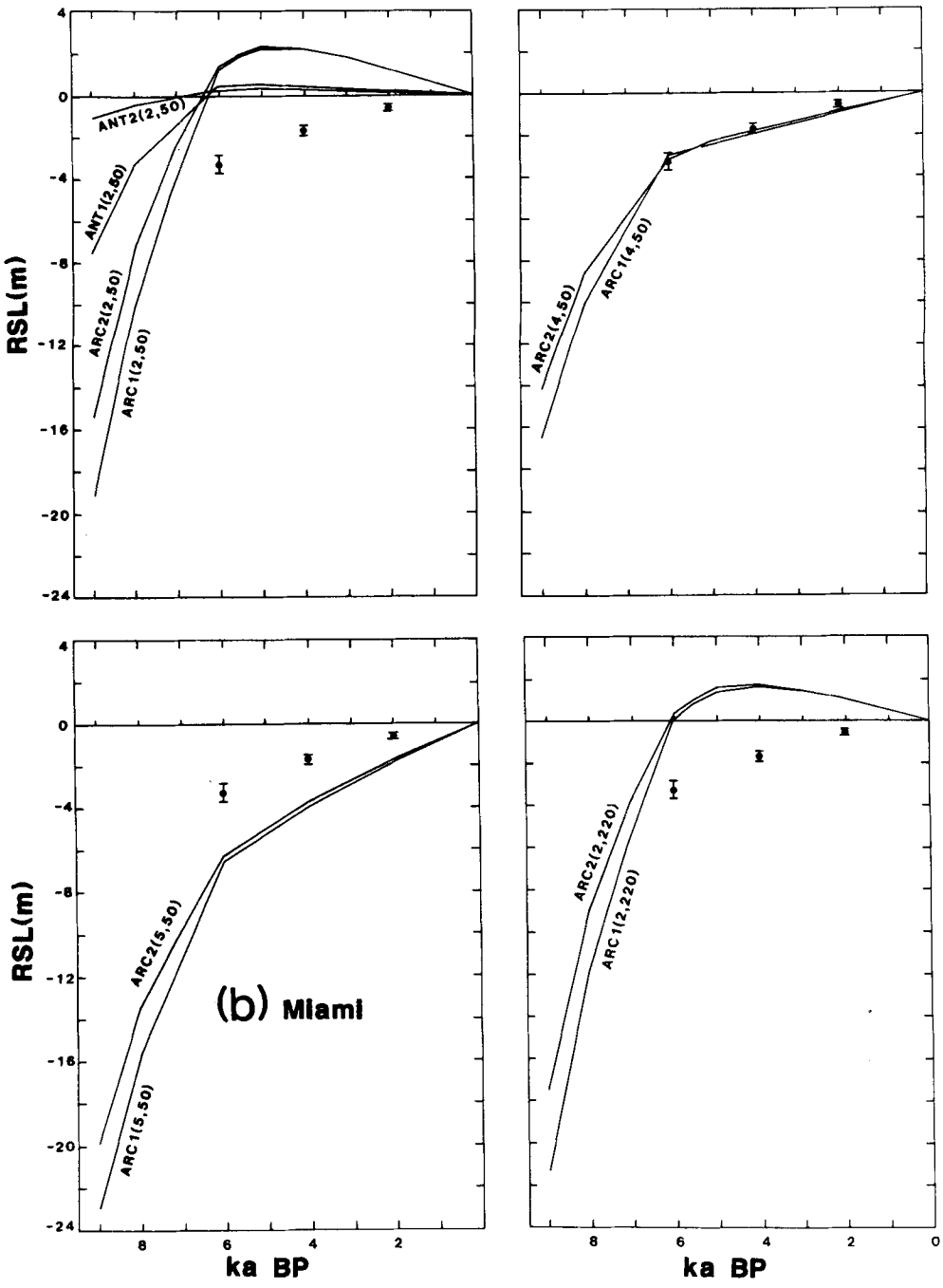

Figure 20 – *continued*

length components than at the central sites. At these edge sites the Antarctic contributions to sea-level become important during the late glacial stage (Fig. 19). At Boston, for example, the ARC 2 and ANT 1 contributions are of similar magnitude but of opposite sign at 10–12 ka BP. The Boston site lies within the limits of the Laurentide ice sheet up to about 12 ka

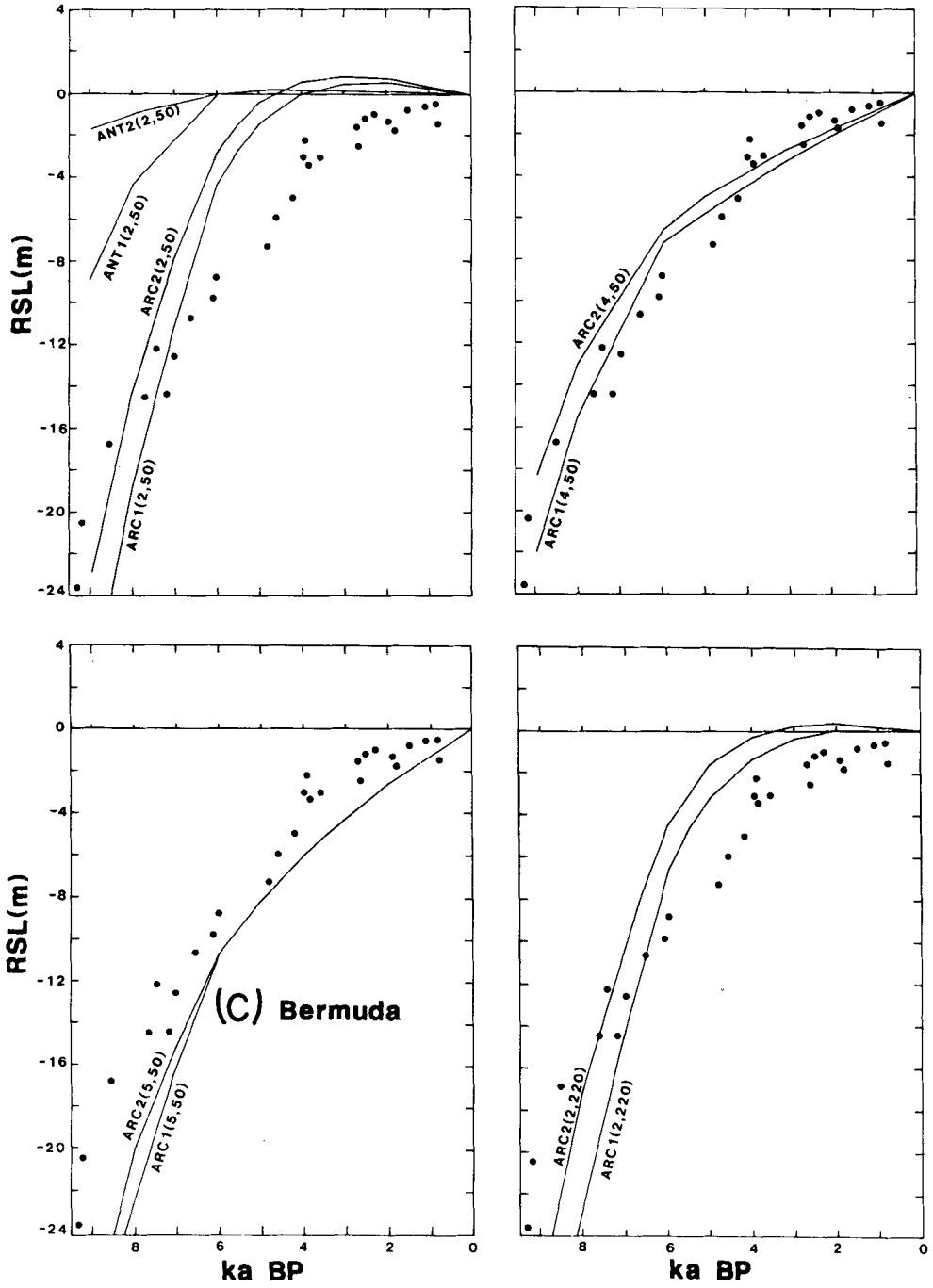

Figure 20 – *continued*

BP and the sea-level responses to the two arctic ice models are quite different (Fig. 19). Likewise, the two melting histories at Newfoundland are distinctly different while at Brigantine, just outside the limit of the ice sheet, the two models are virtually the same. The deformation across the ice-sheet margin is further illustrated in Fig. 22 for sites along the

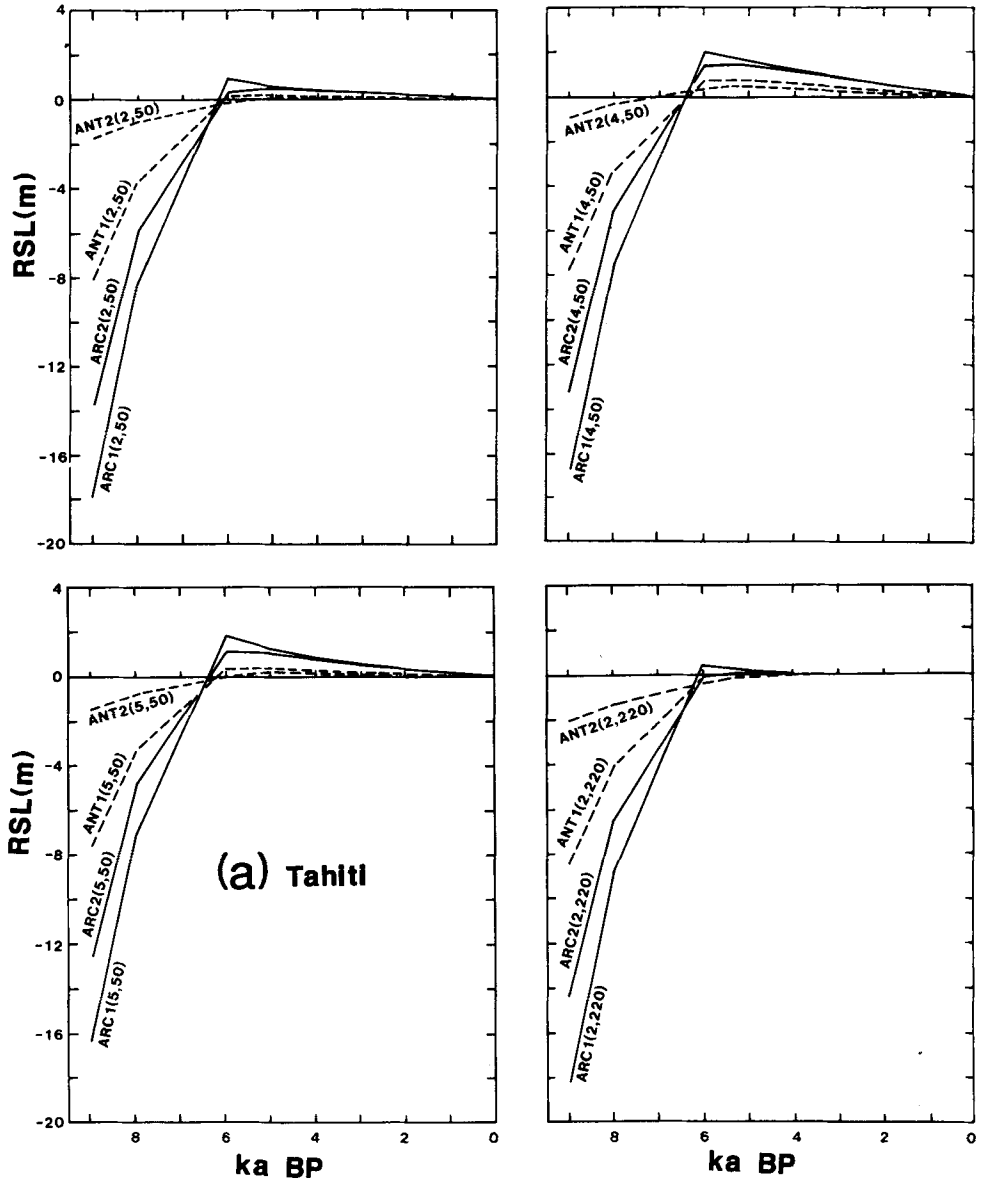

Figure 21. Same as Fig. 18 but for sites in the far-field. (a) Tahiti, (b) Hauraki Gulf, (c) Karumba.

Atlantic shoreline from Maine to Florida at the epochs of 11 ka BP and 6 ka BP. As for the sites within the Laurentide ice sheet, ARC 2 provides better agreement with observations than ARC 1. At Boston, the mantle models (2, 50) and (2, 220) fit the observations about equally well; the Newfoundland data excludes the latter model and the Brigantine observations are better matched by the (2, 220) model than the (2, 50). In general, sea-levels at these sites appear to be unsuitable for estimating mantle structure if major uncertainties about the ice loads remain, as is indeed the case.

Further away from the edge of the ice-sheet limit, the sea-level response is less sensitive to the ice models than to the mantle structure (Fig. 20). Here the model (2, 50), and to a

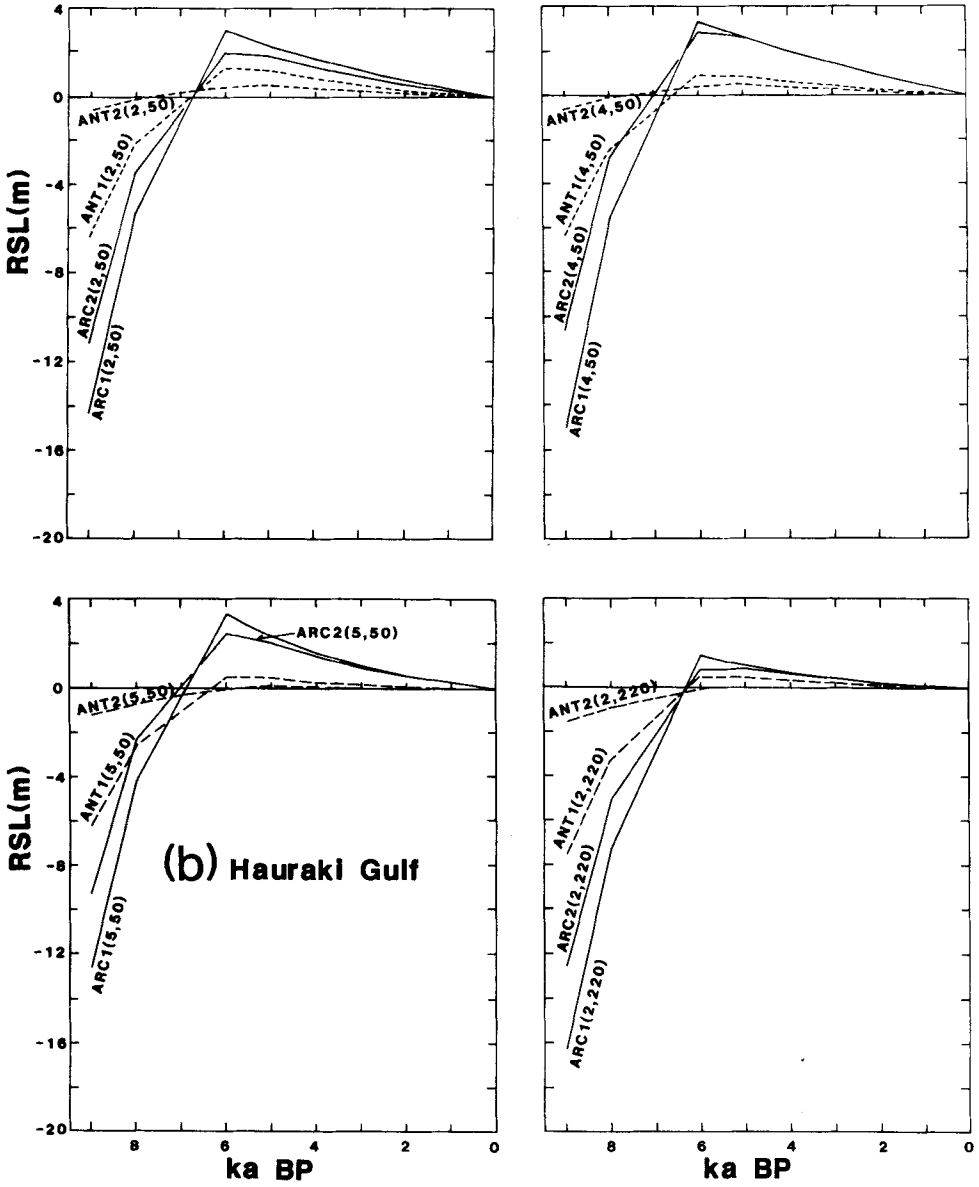

Figure 21 – *continued*

lesser degree (2, 220) appears to be excluded because the predicted Holocene sea-level high-stands are not observed. At these sites, model (4, 50) compares well with the observations. In the far-field the sea-level response is not very sensitive to the details of the Arctic ice load but the potential Antarctic contributions become significant. At these sites a good discriminator for mantle models is the amplitude of sea-level at about 6 ka BP. Here the ice model ARC 1 produces more pronounced Holocene high-stands in sea-level than does the model ARC 2, a consequence of the differences in melting histories of these two models near 6 ka BP. The amplitude of the Holocene high-stand is sensitive to the rate at which melt-

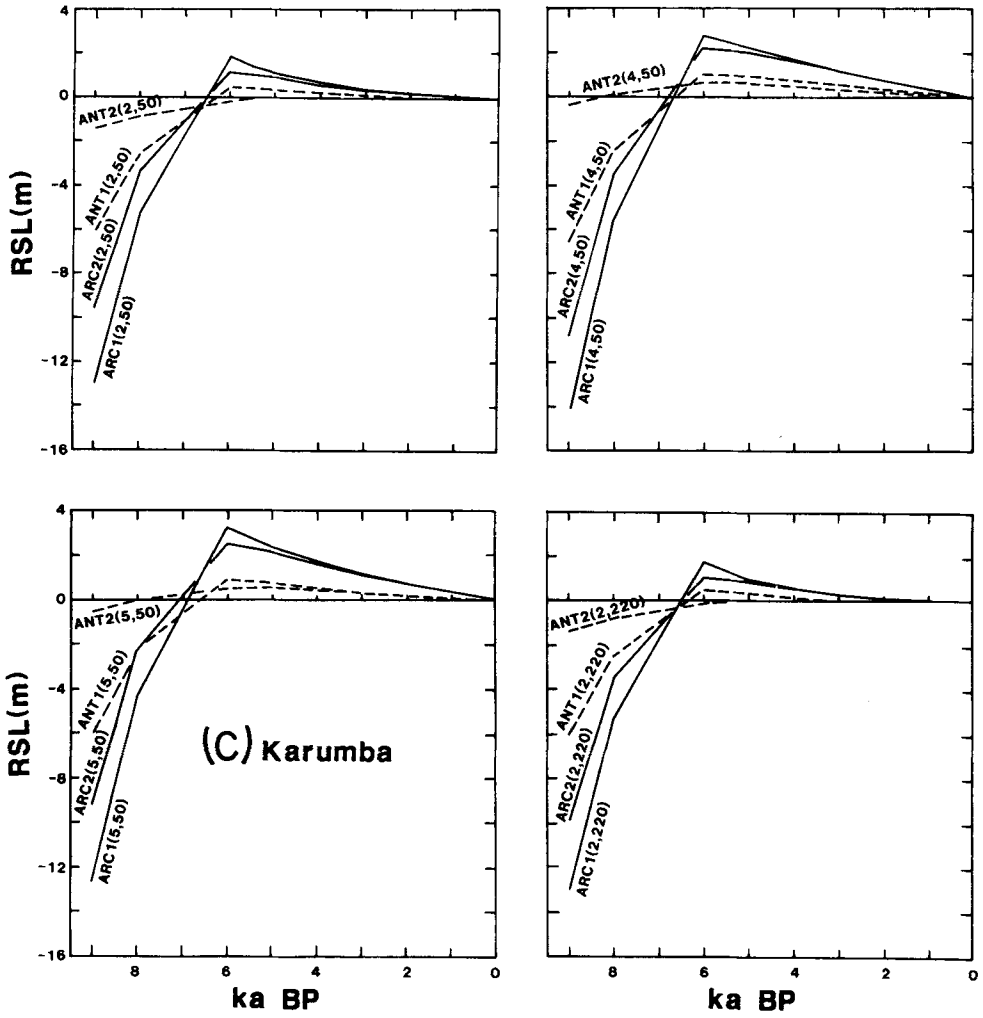

Figure 21 – *continued*

water is added to the oceans during the final stage of deglaciation and, in the interval 6–5 ka BP, this occurs more gradually in model ARC 2 than in ARC 1; The Holocene highs are further augmented by the Antarctic ice load ANT 1 while ANT 2 tends to reduce these heights. In general, the mantle models (2, 50) and (2, 220) produce similar results although the latter produces smaller Holocene high-stands. The models in which viscosity increases with depth tend to produce early Holocene sea-levels that are generally excessive: at Karumba, sea-level at 6 ka BP was about 2 m above the present level (Chappell *et al.* 1982); in French Polynesia Holocene maxima are rarely more than 1 m above present sea-level (e.g. Pirazolli *et al.* 1985) and in the Hauraki Gulf sea-level has been near its present level for about the last 6.5 ka (Gibb 1986).

The ice models discussed so far assume that the maximum extent of the ice sheets was attained sufficiently long ago for the loads to have reached a state of isostatic equilibrium with the Earth by the time the final melting began. From sea-level variations noted by Emery *et al.* (1971), Chappell (1974) and others it appears that there may have been a

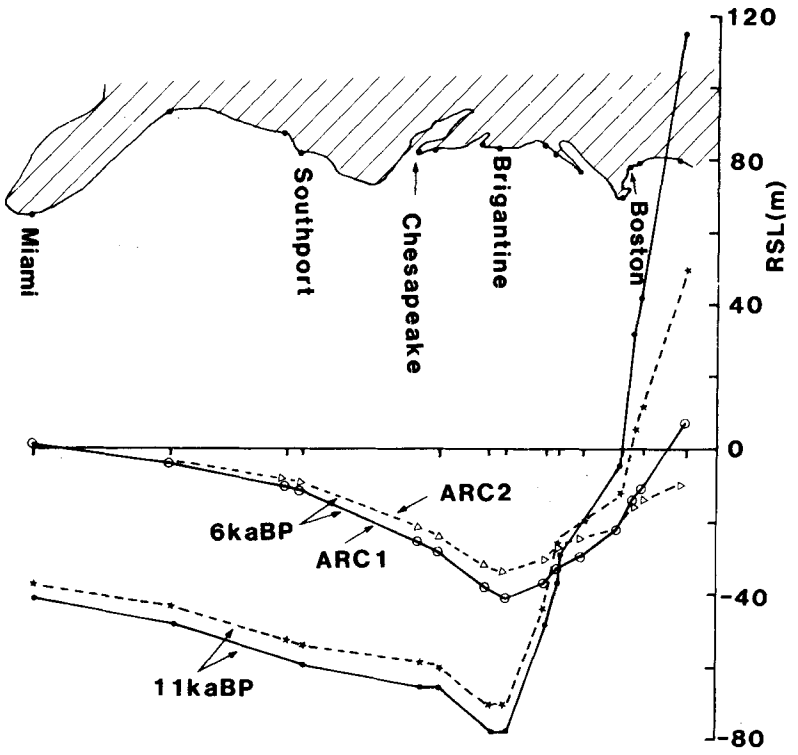

Figure 22. Relative sea-levels along the Atlantic coast of North America at epochs 11 and 6 ka BP for the models ARC 1 (2, 50) and ARC 2 (2, 50).

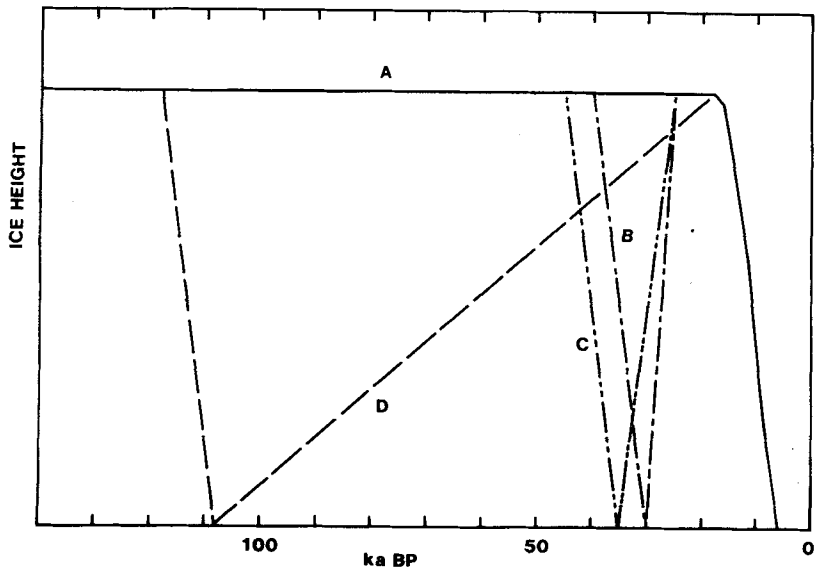

Figure 23. Schematic ice models for earlier cycles of deglaciation. Model A represents case model in which the ice load is assumed to be in isostatic equilibrium with the Earth at the time of melting. B and C represent models with a previous cycle of deglaciation and glaciation at between 45 and 25 ka BP. Prior to this cycle the ice load is assumed to be in isostatic equilibrium. Model D represents the case where the current ice sheet grew slowly to a maximum extent at 18 ka BP. In all models the final deglaciation follows the melt history of model ARC 1.

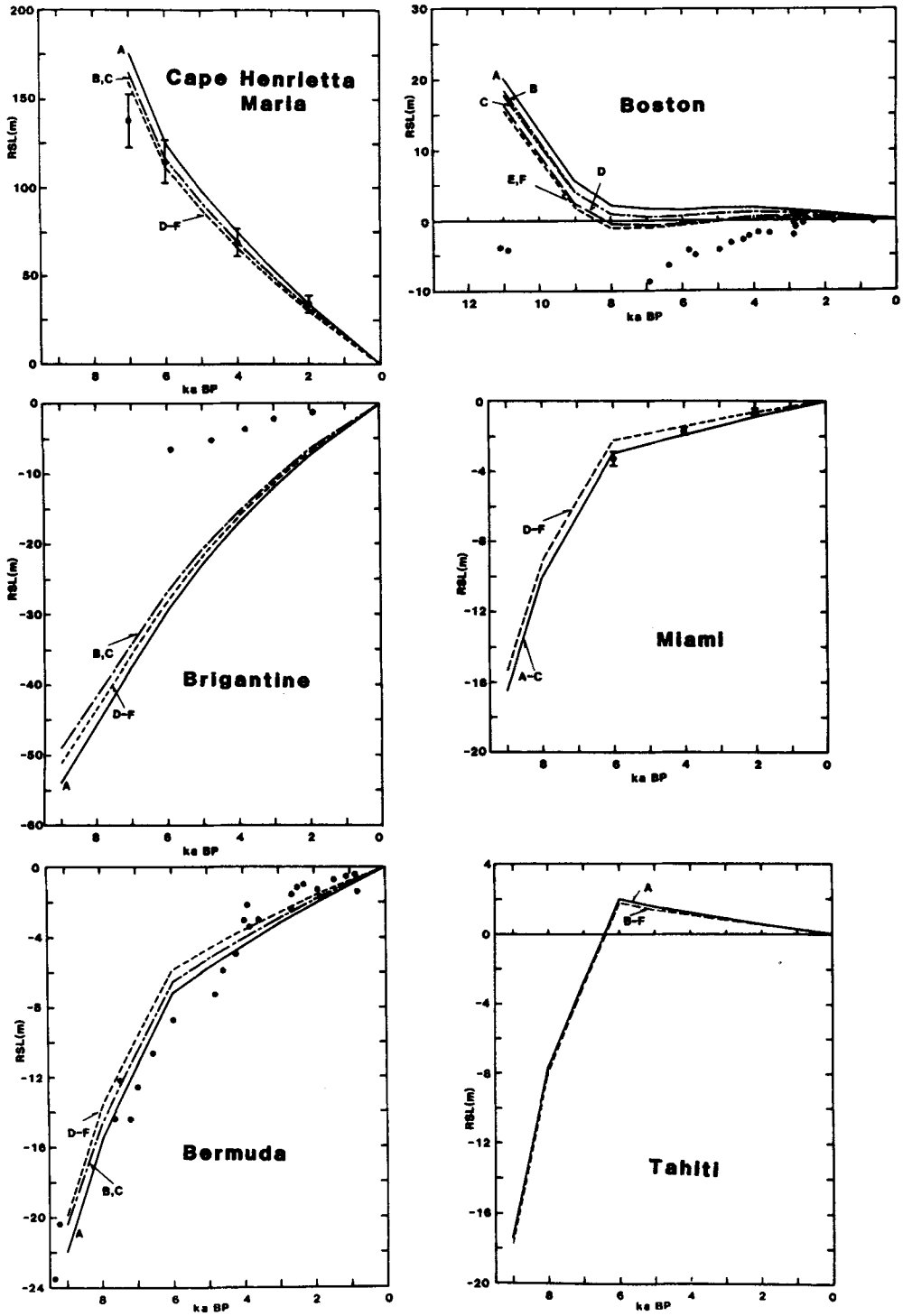

Figure 24. Relative sea-levels predicted for an Earth with viscosity structure according to model 4 and a 50 km thick lithosphere, and for the ice models A–F discussed in text.

relative sea-level high-stand of short duration between 35 and 30 ka BP as well as at earlier times. Thus present sea-level variations may also reflect the mantle response to these earlier cycles of loading and unloading. Fig. 23 illustrates a number of loading histories that account qualitatively for some of the sea-level fluctuations in the past 10^5 yr. Model A corresponds to the ARC 1 model in which the maximum ice load is assumed to have been in place for a sufficiently long period for the local isostatic state to have been achieved. For the earlier cycles, the ice covered area waxes and wanes according to the models B–F by amounts that are proportional to the height of the ice column at 18 ka BP. In models B and C the period of ice-sheet construction between 35 and 30 ka BP was immediately preceded by deglaciation, while in model D the period of construction occurred gradually over 90 ka up to 18 ka BP and then collapsed as before. Models E and F correspond to three and five cycles of model D, respectively.

The response of two mantle models to these longer time-scale loads has been examined, viscosity models 2 and 4, both with a 50 km thick lithosphere, but because the dependence of Holocene sea-levels change on these earlier cycles is essentially independent of mantle models within the range examined here, only the results for model (4, 50) are illustrated in Fig. 24. Within the ice sheet, the differences in the predicted Holocene sea-levels are about 15 m at 7 ka BP, representing about 10 per cent of the observed sea-levels at that time. The effect at Boston, near the edge of the ice sheet, is about 5 m, comparable to the observed sea-level for that epoch. With increasing distance from the ice sheet these differences become less important; see the results for Brigantine, Bermuda, Miami, and the far-field site of Tahiti. In general, the models based on the assumption of the isostatic state having been achieved prior to the last glaciation phase appears adequate for predicting relative sea-level changes during the late- and post-melting phases of unloading. The exceptions to this are sites near the maximum extent of the ice sheets and, as such sites are also very sensitive to the detailed melting history, they are best avoided in studies of the Earth's response to the changing surface loads.

8 Conclusion

We have examined the solution of the equation defining the surface deformation response of a viscoelastic – otherwise Earth-like – planet to surface loads characterized by loading cycles of about 10^4–10^5 yr duration. When applied to the Earth the load is the exchange of mass between the oceans and ice sheets during times of glaciation and deglaciation and the observed response is the change in sea-levels through time, relative to present-day levels. The particular emphasis of this paper has been on the requirements for obtaining convergent solutions for the sea-level changes, rather than on estimating the elastic and anelastic properties that define the planet's response to the loads. These requirements were summarized at the end of Section 6 and the essential result is the need for high degree expansions for both the ice load and the ocean function that specifies the geographic distribution of the meltwater. The degree N_{max} at which convergence of the sea-level equation is obtained is a function of the Earth's response, of the geometry of the ice load, and of the location at which relative sea-level is predicted. For $N_{max} \simeq 36$, for example, the solutions for the sea-level equation at the late stage of deglaciation or during the Holocene do not generally converge, particularly for sites near the edge of the ice sheet at its maximum extent (Figs 8–10). Convergence can be achieved with $N_{max} \simeq 36$, however, if the mantle viscosity is increased or if models with thick ($H \simeq 200$ km) lithospheres are introduced in the Earth's response (Fig. 17).

The 5° ice models that have been used in most studies do not produce convergent

solutions in the near-field because these models contain excessive power in degrees beyond about $N \simeq 30$ (see Fig. 4a). The spatially smoothed ice models of 1° resolution produce better behaved solutions in the near-field, without requiring a thick lithosphere or high mantle-viscosity, although the summations still have to be carried out to high degree; about $N_{max} \simeq 90$ for sites near the ice load (Figs 13, 14). The analysis by Peltier & Andrews (1976) and Wu & Peltier (1983) are based on a finite element approach and their solutions correspond to the above formulation with $N_{max} = \infty$. However, it is important that the resolution of the ice grid is sufficiently small, ideally compatible with $N_{max} = \infty$, when sea-levels are evaluated near the edge of the ice sheets. For example, with the 1° ice model the sites of New York, Clinton and Barnstable lie within or at the edge of the ARC 1 ice sheet at its maximum extent, in agreement with most reconstructions of the ice sheets (see, for example, fig. 13 of Wu & Peltier 1983). With the 5° ice model these sites lie outside the ice sheet. Wu & Peltier (1983) recognized that their 5° ice grid model created a problem with spatial resolution of sea-levels although they do not appear to have investigated this further in their subsequent papers where the mantle response has been inferred from such sites (e.g. Peltier 1984). Quinlan & Beaumont (1981) recognized the need for a higher resolution of the ice models in their rebound calculations for eastern Canada. An estimate of the error incurred by the use of the 5° ice grid follows from a comparison of the solutions for the 1° and 5° models, provided that the former have converged by degree about 90. From Fig. 17, this error at Boston at 6 ka BP, for example, in about 10 m for the model without a lithosphere. For the 220 km thick lithospheric model this error is reduced to about 2 m.

In the far-field, relative sea-levels during the Holocene are generally more sensitive to the Earth's response to the meltwater loading (the ΔZ_2 term in Fig. 15) than to the glacial unloading. Here the details of the geographic distribution of the ice loads are relatively unimportant although the rates of unloading do have an influence on the sea-level curve, including the amplitude of the Holocene high-stands. More important is the representation of the ocean function in the vicinity of the point at which sea-level is predicted and, in regions of complex shorelines or at ocean islands, large N_{max} are required to ensure convergence (Figs 15, 16) unless, as before, the solutions are stabilized by introducing thick lithospheric models or by increasing the mantle viscosity (Fig. 17). This need for a detailed description of the shoreline geometry also raises the question of whether it is necessary to introduce a time-dependent description of this boundary at certain sites. Wu & Peltier's (1983) finite element representation of the ocean geometry is very approximate, ranging from 5° to 20°. In addition, they approximate these areas by equivalent circular disc loads which results in some areas being overloaded and others underloaded. Wu & Peltier have again recognized these restrictions but they do not consider that these limitations are severe. However, the example used in the present studies clearly indicate the inadequacy of such a representation for modelling the Holocene part of the sea-level response.

We have examined in a general way the dependence of the sea-level variations on both ice and earth models, using as examples the sea-levels at a number of sites – ranging from within the ice sheet to the far-field – where relative sea-levels have been observed during the late stages of deglaciation and the Holocene. The sea-level response near the centre of the former Laurentide ice sheet is relatively insensitive to assumptions of lithospheric thickness since the dominant wavelength of the load is considerably greater than the likely effective thickness of the lithosphere. Within the limited range of models examined the observed sea-levels at these sites are about equally sensitive to the choice of ice models as to the choice of mantle models (Fig. 18). Sea-levels at locations near the edge of the former ice sheet vary significantly with changes in the ice models, as well as with changes in the Earth's response, and while uncertainties about the ice models remain, in both the geographic extent and the

time history of melting, sea-levels at these sites are not suitable for estimating the Earth structure. This is well illustrated by the results for Newfoundland (Fig. 19) where the two ice models differ by about 3 ka in the time at which deglaciation terminated. Near-field observations along the Atlantic shoreline of North America are relatively insensitive to the choice of ice models (always within the range of the ARC 1–2 models discussed here) and are more appropriate for estimating mantle structure. At these, and at the ice edge sites, an additional uncertainty arises from the Antarctic contributions to sea-level change during the melting phase. These contributions become increasingly important for sites in the far-field.

Without having examined the full range of Maxwell-viscoelastic mantle models and sea-level observations, our preferred model is one in which the lithosphere need not have a thickness in excess of 80 km, an upper mantle viscosity of about 10^{21} Pa s and a lower mantle viscosity of 10^{21}–10^{23} Pa s. The conclusion on the lithospheric thickness is in contradiction to Peltier's (1984) conclusion in which he argues that the lithospheric thickness is in excess of 200 km. This different conclusion is a consequence of the neglect of Antarctic meltwater and of the inadequate spatial and temporal representation of the ice model adopted by Peltier for sites that lie predominantly near the edge of the ice sheet. Peltier adopts a load defined by

$$L(\alpha, t) = \rho_i h_0 [\alpha_0 - \alpha]^{1/2} f(t),$$

where h_0 is the maximum ice thickness, α_0 is the maximum radius of the ice sheet, α is the distance from the centre of the ice sheet, and $f(t)$ is the time function, and assumes that the final stage of deglaciation occurs instantaneously at 11 ka BP. The best fit between observations and predictions, based on this simple load model and an assumed mantle viscosity of 10^{21} Pa s, is found for a lithospheric thickness of nearly 250 km (see his Fig. 7). In view of the sensitivity of the relative sea-levels to the ice models at sites near the edge of the field, this simple model, while attractive from the viewpoint of giving an intuitive insight into the sea-level response, is quite inadequate for deducing Earth parameters. The results for sea-level near the ice sheet clearly illustrate the dangers inherent in the use of such simplified ice models. Peltier does compute the sea-levels for this earth model using the ICE 2 load, but nothing in his table 1 permits one to conclude that this particular model provides a better fit to the observations than do other plausible models.

Wu & Peltier (1983) have concluded that the lower mantle viscosity is not significantly different from that assumed for the upper mantle, namely 10^{21} Pa s. They reach this conclusion by adopting a 120 km thick lithosphere and an upper mantle viscosity of 10^{21} Pa s and using the 5° representations of the ice loads. Their conclusions are based largely on relative sea-levels observed within and near the edge of the ice sheet, at sites where the response is also sensitive to the ice models. We do not necessarily disagree with their conclusion, but we consider it is not yet a strong enough conclusion to allow meaningful statements about transient rheology to be made as has been done by Peltier (1985) and Sabadini *et al.* (1985).

References

Belperio, A. P., Hails, J. R. & Gostin, V. A., 1983. A review of Holocene sea levels in south Australia, in *Australian Sea Levels in Last 15000 Years: A Review*, pp. 37–47, ed. Hopley, D., James Cook University of North Queensland, Australia.

Bland, D. R., 1960. *The Theory of Linear Viscoelasticity*, Pergamon Press, New York.

Bloom, A. L., 1967. Pleistocene shorelines: a new test of isostasy, *Bull. geol. Soc. Am.*, **78**, 1477–1494.

Broecker, W. S., 1984. Termintions, in *Milankovitch and Climate, Part 2*, ed. Berger, A. L., Reidel, Dordrecht.

Brown, R. G., 1983. Sea level history over the past 15 000 years along the western Australian coastline, in *Australian Sea Levels in the Last 15 000 Years: A Review*, pp. 29–36, ed. Hopley, D., James Cook University of North Queensland, Australia.

Cathles, L. M., 1975. *The Viscosity of the Earth's Mantle*, Princeton University Press, New Jersey.

Cathles, L. M., 1980. Interpretation of postglacial isostatic adjustment phenomena in terms of mantle rheology, in *Earth Rheology, Isostasy and Eustasy*, ed. Mörner, N., Wiley, New York.

Chappell, J., 1974. Geology of coral terraces, Huon Peninsula, New Guinea: a study of Quaternary tectonic movements and sea-level changes, *Bull. geol. Soc. Am.*, **85**, 553–570.

Chappell, J., Rhodes, E. G., Thom, B. G. & Wallensky, E. P., 1982. Hydro-isostasy and the sea-level isobase of 5500 BP in north Queensland, Australia, *Mar. Geol.*, **49**, 81–90.

Clark, J. A. & Lingle, C. S., 1979. Predicted relative sea-level changes (18 000 years BP to present) caused by late glacial retreat of the Antarctic ice sheet, *Quat. Res.*, **11**, 279–298.

Clark, J. A., Farrell, W. E. & Peltier, W. R., 1978. Global changes in postglacial sea level: a numerical calculation, *Quat. Res.*, **9**, 265–287.

Crough, S. T., 1977. Isostatic rebound and power-law flow in the asthenosphere, *Geophys. J. R. astr. Soc.*, **50**, 723–738.

Dahlen, F. A., 1976. The passive influence of the oceans upon the rotation of the Earth, *Geophys. J. R. astr. Soc.*, **46**, 363–406.

Denton, G.. H. & Hughes, T. J. (eds), 1981. *The Last Great Ice Sheets*, Wiley, New York.

Drewry, D. J. (ed), 1982. *Antarctica: Glaciological and Geophysical Folio*, Scot Polar Res. Inst., Cambridge.

Dziewonski, A. M. & Anderson, D. L., 1981. Preliminary reference Earth model, *Phys. Earth planet. Int.*, **25**, 297–356.

Emery, K. O., Niino, H. & Sullivan, B., 1971. Post Pleistocene levels of the East China Sea, in *Late Cenozoic Glacial Ages*, ed. Turekian, K. K., Yale University Press, New Haven.

Fairbridge, R. W., 1961. Eustatic changes in sea level, *Physics Chem. Earth*, **4**, 99–184.

Farrell, W. E. & Clark, J. A., 1976. On postglacial sea-level, *Geophys. J. R. astr. Soc.*, **46**, 647–667.

Gibb, J. G., 1986. A New Zealand Holocene eustatic sea-level curve and its application to determination of vertical tectonic movements, *Bull. R. Soc. N.Z.*, in press.

Gilbert, F. & Dziewonski, A. M., 1975. An application of normal mode theory to the retrieval of structural parameters and source mechanisms from seismic spectra, *Phil. Trans. R. Soc. A*, **278**, 187–269.

Hager, B. H., 1984. Subducted slabs and the geoid: constraint on mantle rheology and flow, *J. geophys. Res.*, **89**, 6003–6015.

Haskell, N. A., 1935. The motion of a viscous fluid under a surface load, *Physics*, **6**, 265–269.

Haskell, N. A., 1936. The motion of a viscous fluid under a surface load, Part II, *Physics*, **7**, 56–61.

Haskell, N. A., 1937. The viscosity of the asthenosphere, *Am. J. Sci.*, **33**, 22–28.

Kaula, W. M., 1980. Problems in understanding vertical movements and Earth rheology, in *Earth Rheology, Isostasy and Eustasy*, pp. 577–588, ed. Mörner, A., Wiley, New York.

Kaye, C. A. & Barghoorn, E. S., 1964. Late Quarternary sea level change and crustal rise at Boston, Massachusetts, with notes on the auto compaction peat, *Bull. geol. Soc. Am.*, **75**, 63–80.

Lambeck, K. & Nakiboglu, S. M., 1980. Seamount loading and stresses in the oceanic lithosphere, *J. geophys. Res.*, **85**, 6403–6418.

Lambeck, K. & Nakada, M., 1985. Holocene fluctuations in sea-level: constraint on mantle viscosity and melt-water sources, *Proc. Fifth Int. Coral Reef Cong., Tahiti*, **3**, 79–84.

Lidén, R., 1938. Senkvartära strandförskjutningens förlopp och Kronologii Ångermand, *Geol. För. Stokh. Förh.*, **60**, (H3), 397–404.

Lliboutry, L. A., 1971. Rheological properties of the asthenosphere from Fennoscandia data, *J. geophys. Res.*, **76**, 1433–1466.

McConnell, R. K., 1965. Isostatic adjustment in a layered Earth, *J. geophys. Res.*, **70**, 5171–5188.

McConnell, R. K., 1968. Viscosity of the mantle from relaxation time spectra of isostatic adjustment, *J. geophys. Res.*, **73**, 7089–7105.

Nakada, M., 1983. Rheological structure of the Earth's mantle derived from the glacial rebound in Laurentide, *J. Phys. Earth*, **31**, 349–386.

Nakada, M., 1986. Holocene sea levels in oceanic islands: implications for the rheological structure of the earth's mantle, *Tectonophys.*, **121**, 263–276.

Nakiboglu, S. M., Lambeck, K. & Aharon, P., 1983. Postglacial sealevels in the Pacific: implications with respect to deglaciation regime and local tectonics, *Tectonophys.*, **91**, 335–358.

Newmann, C. A., 1971. Quaternary sea level data from Bermuda, *Quaternaria*, **XIV**, 41–44.

Newman, W. S., Cinquemani, L. J., Pardi, R. R. & Marcus, L. F., 1980. Holocene delevelling of the United States' east coast, in *Earth Rheology, Isostasy and Eustasy*, ed. Mörner, N., Wiley, New York.

Niskannen, E., 1948. On the viscosity of the Earth's interior and crust, *Ann. Acad. Sci. Fennicae*, **15**, (A), 1–28.

Paterson, W. S. B., 1972. Laurentide ice sheet: estimated volumes during late Wisconsin, *Rev. Geophys. Space Phys.*, **10**, 885–917.

Peltier, W. R., 1974. The impulse response of a Maxwell earth, *Rev. Geophys. Space Phys.*, **12**, 649–669.

Peltier, W. R., 1984. The thickness of the continental lithosphere, *J. geophys. Res.*, **89**, 11 303–11 316.

Peltier, W. R., 1985. New constraint on transient lower mantle rheology and internal mantle buoyancy from glacial rebound data, *Nature*, **318**, 614–617.

Peltier, W. R. & Andrews, J. T., 1976. Glacial isostatic adjustment – I: The forward problem, *Geophys. J. R. astr. Soc.*, **46**, 605–646.

Peltier, W. R., Farrell, W. E. & Clark, J. A., 1978. Glacial isostasy and relative sea level: a global finite element model, *Tectonophys.*, **46**, 81–110.

Pirazzoli, P. A., Montaggioni, L. F., Delibrias, G., Faure, G. & Salvat, B., 1985. Late Holocene sea-level changes in the Society Islands and in the northwest Tuamoto atolls, *Proc. Fifth Int. Coral Reef Congr. Tahiti*, **3**, 131–134.

Post, R. L. & Griggs, D. T., 1973. The Earth's mantle: evidence of non-Newtonian flow, *Science*, **181**, 1242–1244.

Quinlan, G. & Beaumont, C., 1981. A comparison of observed and theoretical postglacial relative sea level in Atlantic Canada, *Can. J. Earth Sci.*, **18**, 1146–1163.

Quinlan, G. & Beaumont, C., 1982. The deglaciation of Atlantic Canada as reconstructed from the post-glacial relative sea-level record, *Can. J. Earth. Sci.*, **19**, 2232–2246.

Richards, M. A. & Hager, B. H., 1984. Geoid anomalies in a dynamic Earth, *J. geophys. Phys.*, **89**, 5987–6002.

Sabadini, R., Yuen, D. A. & Gasperini, P., 1985. The effects of transient rheology on the interpretation of lower mantle viscosity, *Geophys. Res. Lett.*, **12**, 361–365.

Schwiderski, E. W., 1978. *Hydrodynamically Defined Ocean Bathymetry*, Naval Surface Weapons Center, Dahegren, Virginia.

Shepard, F. P., 1963. Thirty-five thousand years of sea level, in *Essays in Marine Geology in Honor of K. O. Emery*, pp. 1–10, eds Clements, T., Stevenson, R. & Halmos, D., University of Southern California Press, Los Angeles.

Stoddart, D. R., Spencer, T. & Scoffin, T. P., 1985. Reef growth and karst erosion on Mangaia, Cook Islands: a reinterpretation, *Z. Geomorph. N.F., Suppl.*, **57**, 121–140.

Stuiver, M., Denton, G. H., Hughes, T. J. & Fastook, J. L., 1981. History of the marine ice sheet in west Antarctica during the last glaciation: a working hypothesis, in *The Last Great Ice Sheets*, eds Denton, G. H. & Hughes, T. J., Wiley, New York.

Sugimura, A., 1977. Ice sheets, continents and oceans, *Kagaku*, **47**, 749–755 [in Japanese].

Takeuchi, H. & Hasegawa, Y., 1965. Viscosity distribution within the Earth, *Geophys. J. R. astr. Soc.*, **9**, 503–508.

US Navy, 1985. *Navy 10' Elevation Data*, US Navy.

Van Bemmelen, R. W. & Berlage, H. P., 1935. Versuch Einer Mathmatischen Besonderor Berucksichtegung der Undationstheorie, *Beitr. Geophys.*, **43**, 19–55.

Vening Heinesz, F. A., 1937. The determination of the Earth's plasticity from the post-glacial uplift of Scandinavia: isostatic adjustment, *Ned. Akad: Wetenschaphen Proc. 2nd Ser.*, **40**, 654–662.

Walcott, R. I., 1972. Late Quarternary vertical movements in eastern America: quantitative evidence of glacio-isostatic rebound, *Rev. Geophys. Space Phys.*, **10**, 849–884.

Walcott, R. I., 1973. Structure of the Earth from glacio-isostatic rebound, in *Annual Review of Earth and Planetary Sciences*, pp. 15–37, ed. Donath, F. A., Palo Alto. Annual Reviews Inc., California.

Walcott, R. I., 1980. Rheological models and observational data of glacio-isostatic rebound, in *Earth Rheology, Isostasy and Eustasy*, ed. Mörner, N., Wiley, New York.

Wu, P. & Peltier, W. P., 1982. Viscous gravitational relaxation, *Geophys. J. R. astr. Soc.*, **70**, 435–485.

Wu, P. & Peltier, W. R., 1983. Glacial isostatic adjustment and the free air gravity anomaly as a constraint on deep mantle viscosity, *Geophys. J. R. astr. Soc.*, **74**, 377–449.

Yokokura, T. & Saito, M., 1978. Viscosity of the upper mantle as non-Newtonian fluid, *J. Phys. Earth*, **26**, 147–166.

Yonekura, N., Matsushima, Y., Maeda, Y. & Kayane, H., 1984. Holocene sea-level changes in the southern Cook Islands, in *Sealevel Changes and Tectonics in the Middle Pacific*, pp. 113–133, Rept. HIPAC Project, Kobe University, Japan.

Appendix 1

Consider a load, of radius r_0, density ρ_c, land height h, resting on an elastic lithosphere of flexural rigidity D from time $t = 0$ to $t = t_0$ where t_0 is of the order 10 ka. For simplicity we consider an infinite half-space model in which the lithosphere overlies a purely viscous medium of viscosity η. The force due to the load is

$$F_l = \begin{cases} \rho_c g h f(t), & 0 \leq r \leq r_0 \\ 0 & r > r_0 \end{cases}, \tag{A1}$$

where

$$f(t) = \begin{cases} t/t_0, & 0 \leq t \leq t_0 \\ 1, & t > t_0 \end{cases}. \tag{A2}$$

The force due to the flexure of the elastic plate is

$$F_e = D\left(\frac{d^2}{dr^2} + \frac{1}{r}\frac{d}{dr}\right) w(r, t), \tag{A3}$$

where $w(r, t)$ is the vertical displacement of the plate. The buoyancy force F_b due to the deflection is

$$F_b = \rho_m g w(r, t), \tag{A4}$$

where ρ_m is the density of the viscous layer. The equation for force balance is

$$F_v = F_l + F_e + F_b, \tag{A5}$$

where F_v is the viscous force due to the flow in the mantle induced by the deformation. Taking the zero-order Hankel transform we obtain (Cathles 1975)

$$\hat{F}_v = -\frac{\rho_m g}{\tau(k)}\frac{d\hat{w}}{dt}(k, t), \tag{A6}$$

where $\hat{}$ and k denote the Hankel transform and Hankel parameter, respectively. The relaxation function τ is a function of k and is given by (Haskell 1935, 1936)

$$\tau = \rho_m g / 2\eta k. \tag{A7}$$

Applying the Hankel transform to the other quantities in (A5) gives

$$\frac{d\hat{w}}{dt} = -\tau(k)\left[\left(1 + \frac{Dk^4}{\rho_m g}\right)\hat{w} + \frac{r_0 \rho_c h}{k\rho_m} J_1(kr_0) f(t)\right], \tag{A8}$$

where J_i is the ith order Bessel function. When $t \to \infty$ this equation reduces to the loading equation of an elastic layer over an inviscid medium (e.g. Lambeck & Nakiboglu 1980). With

the load history (A2) the solution of A8 is

$$w(r, t) = \int_0^\infty kJ_0(kr)\hat{w}(k, t)\, dk, \tag{A9}$$

where

$$\left.\begin{aligned} \hat{w}(k, t) &= -\frac{A(k)}{\alpha(k)}\left(1 + \frac{1}{\tau(k)\,\alpha(k)\,t_0}\,[\![\exp[-\tau(k)\,\alpha(k)\,t] - \exp[-\tau(k)\,\alpha(k)\,(t - t_0)]]\!]\right) \\ \alpha(k) &= 1 + \frac{Dk^4}{\rho_m g} \\ A(k) &= \frac{r_0\rho_c h}{k\rho_m} J_1(kr_0). \end{aligned}\right\} \tag{A10}$$

The difference in the deformation at $r = r_0$ between t_0 and $t^*(> t_0)$, corresponding to the definition of the relative sea-level variation (37), follows from (A9) as

$$\Delta w(r_0, t^*, t_0) = -\frac{r_0\rho_c h}{\rho_m}\int_0^\infty G(k)\, dk, \tag{A11}$$

where

$$G(k) = \frac{J_0(kr_0)\,J_1(kr_0)}{\tau\alpha^2 t_0}\,[\![\exp(-\tau\alpha t^*) - \exp[-\tau\alpha(t^* - t_0)] - \exp(-\tau\alpha t_0) + 1]\!]. \tag{A12}$$

With $t^* = 18$ ka, corresponding to the present, and $t_0 = 12$ ka, corresponding to 6 ka BP, equations (A11) and (A12) specify the relative sea-level at 6.0 ka BP.

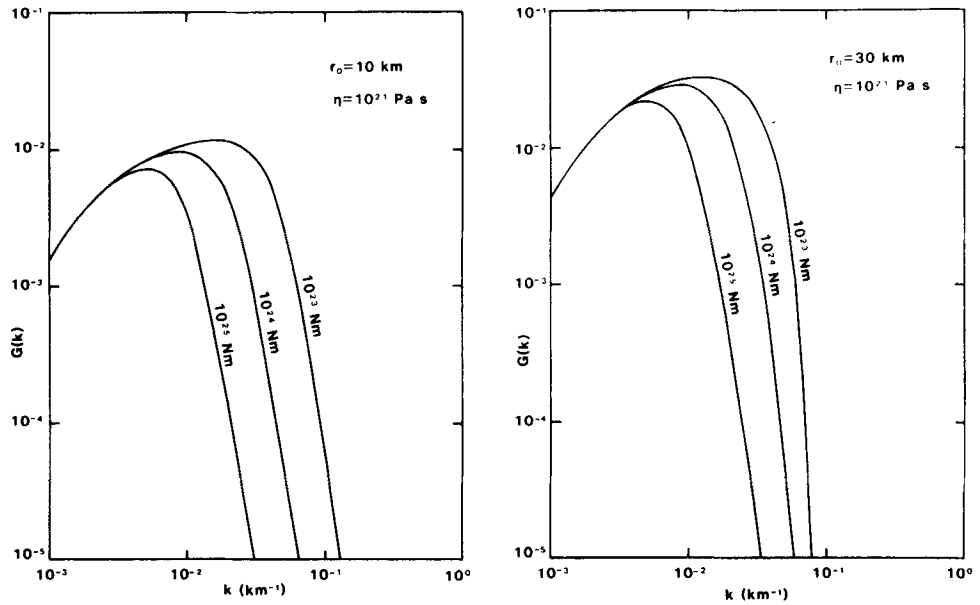

Figure A1. $G(k)$ of equation (A12) as a function of r_0 and D for a viscosity of 10^{21} Pa s.

Fig. A1 illustrates the function $G(k)$ for $\eta = 10^{21}$ Pa s and radii $r_0 = 10$ and 30 km, respectively. These examples illustrate clearly that the contribution to the integral in equation (A11) from small wavenumbers becomes increasingly important as the effective flexural rigidity (or equivalently the thickness of the elastic layer) is decreased; as H, the thickness of the layer, is decreased so is the maximum required k increased. We define a quantity $P(k_c)$ by

$$P(k_c) = \int_{10^{-3}}^{k_c} G(k)\, dk \tag{A13}$$

which can be used to estimate the maximum wavenumber required to ensure an adequate integration of the equation (A11) for specified r_0 and D.

Fig. A2 gives results for $P(k_c)$ as a function of r_0 and D for a viscosity of 10^{21} Pa s. For $r_0 = 50$ km, characteristic of the island of Tahiti, we require $k_c = 3 \times 10^{-2}$ km^{-1} for convergence to be achieved for a lithospheric thickness of about 50 km. For a thinner layer, k_c will be increased. In the spherical coordinate system this means that if $N_{max} \simeq 180$, convergence is achieved only at sites whose coastline geometry is characterized by wavelengths greater than about 200 km and only then if a lithospheric thickness of about 50 km is introduced.

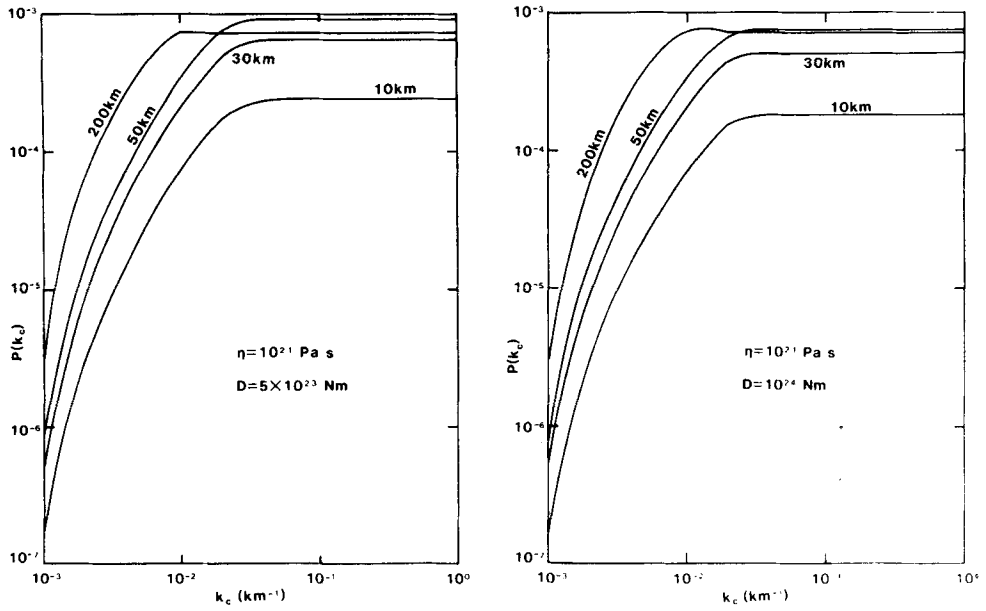

Figure A2. Results for $P(k_c)$ as a function r_0 and D for a viscosity of 10^{21} Pa s.